

# Coordinates

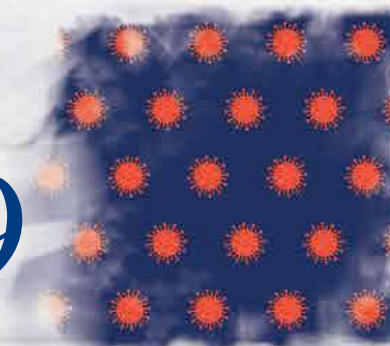
Volume XVII, Issue 2, February 2021

THE MONTHLY MAGAZINE ON POSITIONING, NAVIGATION AND BEYOND

A Power-Law-based approach to

## mapping COVID-19 cases

in the United States



Coverage and optimal visibility-based navigation using visibility analysis



**0.05°**  
ATTITUDE

**0.02°**  
HEADING

**1 cm**  
POSITION

## NEW ELLIPSE-D

### The Smallest Dual Frequency & Dual Antenna INS/GNSS

- » RTK Centimetric Position
- » Quad Constellations
- » Post-processing Software



**Ellipse-D**  
RTK Dual Antenna



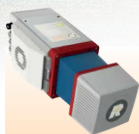
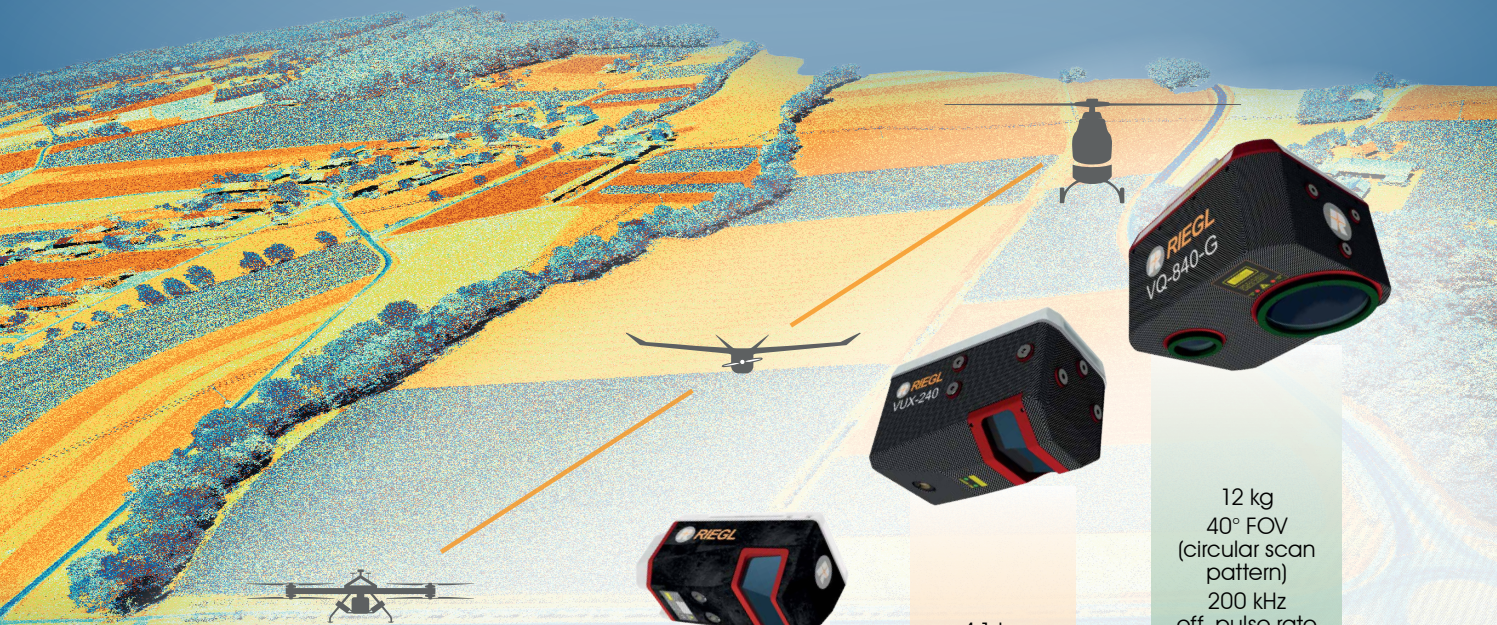
**Ellipse-N**  
RTK Single Antenna



**OEM**  
RTK Best-in-class SWaP-C

# RIEGL WAVEFORM LIDAR FOR UAV-BASED SURVEYING

DISTRIBUTED, SUPPORTED AND SERVICED BY  
**RICOPTER**<sup>®</sup>  
... A RIEGL<sup>®</sup> COMPANY



1.6 kg  
360° FOV  
100 / 200 kHz  
eff. pulse rate  
*extremely lightweight*



3.5 kg  
330° FOV  
500 / 750 kHz  
eff. pulse rate  
*powerful sensor for various applications in wide area UAV surveying*



2.0 kg  
100° FOV  
1.5 MHz  
eff. pulse rate  
*NFB (Nadir/ Forward/ Backward) Scanning for an optimal coverage of complex and vertical targets*



4.1 kg  
75° FOV  
1.5 MHz  
eff. pulse rate  
*versatile scanner for use on high-speed UAVs, helicopters or small manned aeroplanes*



12 kg  
40° FOV  
(circular scan pattern)  
200 kHz  
eff. pulse rate  
water penetration  
2 Secchi depths  
*for topo-bathymetric LIDAR applications*  
*efficient high resolution coastline or shallow water surveying*

## miniVUX-1 / 2 / 3UAV

for applications using low-flying small or mid-sized multi-rotor UAVs  
e.g. mining, topography, forestry, landslide and avalanche monitoring

## VUX-1UAV / -1LR

for applications using fixed-wing UAVs  
e.g. corridor mapping, city modeling

## VUX-120

## VUX-240

for applications using higher-flying large UAVs or helicopters  
e.g. mapping with the need of detailed high-resolution data

## VQ-840-G



Explore the full portfolio of proven RIEGL LIDAR sensors and systems  
[www.riegl.com](http://www.riegl.com)





# In this issue

Coordinates Volume 17, Issue 2, February 2021

## Articles

- A Power-Law-based approach to mapping COVID-19 cases in the United States** BIN JIANG AND CHRIS DE RIJKE 6 **Coverage and optimal visibility-based navigation using visibility analysis from geospatial data** OREN GAL AND YERACH DOYTSHER 12 **Lessons learned from the modernization of the Greek cadastre – Principles and progress** ARISTEA IOANNIDI AND MARIA FOUSKOLAGOUDAKI 22 **Guidelines for acquiring and producing Geospatial Data and Geospatial Data Services including Maps** 26

## Columns

**My Coordinates** EDITORIAL 5 **Old Coordinates** 30 **News** GNSS 31 GIS 33 IMAGING 34 LBS 36 INDUSTRY 36

This issue has been made possible by the support and good wishes of the following individuals and companies

Aristea Ioannidi, Bin Jiang, Chris de Rijke, Maria Fouskolagoudaki, Oren Gal and Yerach Doytsher, Labsat, Riegl, SBG System and many others.

### Mailing Address

A 002, Mansara Apartments  
C 9, Vasundhara Enclave  
Delhi 110 096, India.

**Phones** +91 11 42153861, 98102 33422, 98107 24567

### Email

[information] [talktous@mycoordinates.org](mailto:talktous@mycoordinates.org)

[editorial] [bal@mycoordinates.org](mailto:bal@mycoordinates.org)

[advertising] [sam@mycoordinates.org](mailto:sam@mycoordinates.org)

[subscriptions] [iwant@mycoordinates.org](mailto:iwant@mycoordinates.org)

**Web** [www.mycoordinates.org](http://www.mycoordinates.org)

Coordinates is an initiative of CMPL that aims to broaden the scope of positioning, navigation and related technologies.

CMPL does not necessarily subscribe to the views expressed by the authors in this magazine and may not be held liable for any losses caused directly or indirectly due to the information provided herein. © CMPL, 2021. Reprinting with permission is encouraged; contact the editor for details.

**Annual subscription** (12 issues)

[India] Rs.1,800 [Overseas] US\$100

**Printed and published** by Sanjay Malaviya on behalf of Coordinates Media Pvt Ltd

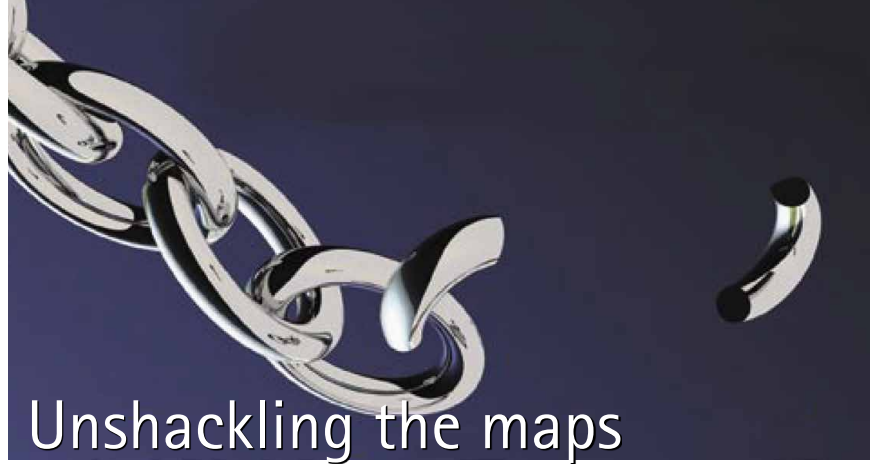
**Published** at A 002 Mansara Apartments, Vasundhara Enclave, Delhi 110096, India.

**Printed** at Thomson Press (India) Ltd, Mathura Road, Faridabad, India

**Editor** Bal Krishna

**Owner** Coordinates Media Pvt Ltd (CMPL)

This issue of Coordinates is of 40 pages, including cover.



# Unshackling the maps

‘What is readily available globally does not need to be regulated’,

So says, the ‘Guidelines for acquiring and producing Geospatial Data and Geospatial Data Services including Maps’ released by the Government of India on Feb 15, 2021. (page 26)

This has been said many times for the last so many years,

By many who relentlessly kept advocating and demanding

To unleash the potential of geospatial data for developmental purposes.

However, such arguments were nixed,

And easily nixed by the ‘security concerns’ – an arena of ‘no go’.

Unlike the earlier policy push which have been over-cautious,

The proposed guidelines are groundbreaking in several ways;

It recognizes the futility of insistence on the continuation of colonial mindset,

It fundamentally changes the approach from ‘all restricted’ to ‘all permitted’ unless stated otherwise.

Bal Krishna, Editor  
bal@mycoordinates.org

**ADVISORS** Naser El-Sheimy PEng, CRC Professor, Department of Geomatics Engineering, The University of Calgary Canada, George Cho Professor in GIS and the Law, University of Canberra, Australia, Professor Abbas Rajabifard Director, Centre for SDI and Land Administration, University of Melbourne, Australia, Luiz Paulo Souto Fortes PhD Associate Professor, University of State of Rio Janeiro (UERJ), Brazil, John Hannah Professor, School of Surveying, University of Otago, New Zealand

# A Power-Law-based approach to mapping COVID-19 cases in the United States

Mapping the ht-index of COVID-19 cases against that of populations shows that the pandemic is largely shaped by the underlying population with the R-square value between infection and population up to 0.82



**Bin Jiang**  
Faculty of Engineering and Sustainable Development, Division of GIScience  
University of Gävle, SE-801 76 Gävle, Sweden



**Chris de Rijke**  
Faculty of Engineering and Sustainable Development, Division of GIScience  
University of Gävle, SE-801 76 Gävle, Sweden

This paper examines the spatial and temporal distribution of all COVID-19 cases from January to June 2020 against the underlying distribution of population in the United States. It is found that, as time passes, COVID-19 cases become a power law with cut-off, resembling the underlying spatial distribution of populations. The power law implies that many states and counties have a low number of cases, while only a few highly populated states and counties have a high number of cases. To further differentiate patterns between the underlying populations and COVID-19 cases, we derived their inherent hierarchy or spatial heterogeneity characterized by the ht-index. We found that the ht-index of COVID-19 cases persistently approaches that of the populations; that is, 5 and 7 at the state and county levels, respectively. Mapping the ht-index of COVID-19 cases against that of populations shows that the pandemic is largely shaped by the underlying population with the R-square value between infection and population up to 0.82.

the situation is still developing. How to better understand the spread mechanisms of the coronavirus in space and over time across different levels of scale concerns many scientists such as geographers, cartographers, and epidemiologists. Many previous studies have already examined the spatial distribution of COVID-19 cases using conventional geographic information systems (GIS) and mapping methods such as hotspot and time series analyses (ESRI 2020). These methods are developed essentially under Gaussian statistics (Jiang 2015) with the assumption that data varies around a characteristic mean (e.g., 1.75 meters as the characteristic mean for human height). A common problem of these methods is that the resulting spatial patterns are sensitive to human subjective decisions like parameter settings. For example, either the number of classes or class intervals has to be decided subjectively. In contrast, we adopt a power-law-based approach under Paretian statistics for examining spatial and temporal distribution of COVID-19 cases in the United States.

We examine the spatiotemporal distribution of all COVID-19 cases in the US across multiple scales of space and time. In space, there are two levels of scale – state and county – whereas over time there are three levels: monthly, weekly, and daily. We detected a power law distribution ( $y = kx^{-a} + m$ , where  $a$  is called power law exponent between 1 and 3, and  $k$  and  $m$  are two constants.)

## Highlights:

- (1) *A statistical physics approach to mapping COVID-19 cases or other dynamic phenomena*
- (2) *This is a timely research work that may be of value for combating the COVID-19 pandemic*
- (3) *The pandemic is largely shaped by the underlying distribution of population*
- (4) *The ht-index is a better indicator than the power law exponent for characterizing the hierarchy*

## Introduction

The novel coronavirus COVID-19 has rapidly spread around the world and triggered an unprecedented pandemic in the few months since January 2020. At the time of writing this paper, over 34.2 million people globally had been infected, with over 1 million deaths, and

for each of three parameters: population, infection, and death. All these three parameters demonstrate power laws with cut-off, despite of some fluctuations for both infection and death. The power law indicates that these three parameters bear an inherent hierarchy or spatial heterogeneity, with far more small events than large ones. To derive this hierarchy, we used head/tail breaks (Jiang 2013) so that each state or county is assigned a ht-index for each of these three parameters to indicate its hierarchical level. The derived hierarchical levels provide new insights into the development of the pandemic for individual states and counties relative to their populations. For example, the pandemic is largely shaped by the underlying population with the R-square value between infection and population up to 0.82. The power-law-based approach enables us to see spatiotemporal patterns that the conventional methods are unable to discover.

The approach has a profound implication on power-law-related research in terms of whether data exhibits a power law or any other similar distribution. That is, from a dynamic view, power law is usually observed when a complex system is fully developed, before which the system is likely to exhibit other less-power-law distributions such as lognormal and exponential. For example, there is little doubt that a tree as a complex biological system demonstrates a power law distribution for its trunk, branches, and leaves, because there are far more leaves than branches, and far more branches than trunk. However, the tree is unlikely to hold a power law at the stage of the germination of the seed. We will further discuss this implication before the conclusion.

The remainder of this paper is structured as follows. Section 2 introduces the data source initially collected by Johns Hopkins University, and the head/tail breaks illustrated by a simple example of the 10 numbers. The power law detection is based on the maximum likelihood method (Clauset et al. 2009), arguably the most robust statistical test. Section 3 presents our results and discussion,

as well as an animation map (<http://lifegis.hig.se/COVID19/>). Section 4 highlights the implication we briefly mentioned above. Finally, Section 5 draws a conclusion of this paper and points to possible future work.

## Data source and methodology

Over three million people have been infected and 208,000 people have died from COVID-19 in the US from January to June of 2020. Johns Hopkins University (2020) has gathered this data and published it on the GitHub website. This data is compared with the country's population at both state and county levels. In general, the two parameters – infection and death – are highly related to population. Like the population in the US, the numbers of infection and death are highly concentrated in a few well-populated states and counties. In this study, we intend to compare COVID-19 cases against the underlying population, in order to develop new insights into spatiotemporal patterns of the pandemic from the multiple scales of space and time.

Like all countries, the US population is not evenly distributed, and it has a very high degree of concentration in a few cities, states, or counties, the so-called inherent hierarchy or spatial heterogeneity. At the city level, this kind of spatial distribution is usually characterized by a power law distribution, such as Zipf's law (1949). Zipf's law states that in terms of population the first largest city is twice as big as the second largest, three times

as big as the third largest and so on. At the county level, the top 20% counties accommodate 80% of the population – the so-called 80/20 principle (Koch 1998) that is credited to the Italian economist and polymath Vilfredo Pareto (1848–1923). What is behind Zipf's law and the 80/20 principle – or the power law in general – is the inherent hierarchy or spatial heterogeneity, which can be illustrated through the head/tail breaks classification scheme (Jiang 2013). This is a recursive function that can be used to derive the inherent hierarchy of data with a heavy-tailed distribution. The derived hierarchical levels or classes reflect the recurrence of far more small numbers than large ones, or spatial heterogeneity, characterized by the ht-index (Jiang and Yin 2014).

Unlike conventional classification methods, with which the number of classes or class intervals are subjectively determined, head/tail breaks adopts the wisdom of crowds thinking (Surowiecki 2004), through which both the number of classes and class intervals are objectively determined by the data; in other words, the data speaks for itself. Head/tail breaks is recursive function, through which a dataset is conceived as the head of the head and so on, and all the tails and the last head constitute the derived classes or inherent hierarchical levels.

To further illustrate the recursive function, let us use a simple example of the 10 numbers (1, 1/2, 1/3, ... 1/10), which follow exactly a rank-size distribution in the so called rank-size plot in which the x-axis is rank, while the y-axis is size.

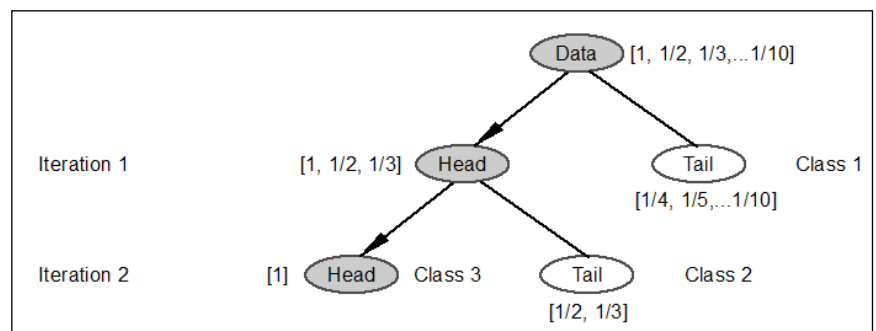


**Figure 1: Illustration of head/tail breaks classification with a simple example of the 10 numbers. (Note: The 10 numbers [1, 1/2, 1/3, ..., 1/10] are classified into three classes: [1/4, 1/5, ..., 1/10], [1/2, 1/3], and [1], which can be said to have three inherent hierarchical levels.)**

Strictly speaking, these 10 numbers cannot be said to be distributed according to Zipf's law, for it is a statistical regularity. Instead these 10 numbers ( $1 + \epsilon_1, 1/2 + \epsilon_2, 1/3 + \epsilon_3, \dots, 1/10 + \epsilon_{10}$ ) (where  $\epsilon$  is a very small value epsilon) are said to fit Zipf's law. Back to the first 10 numbers (Figure 1, Jiang and Slocum 2020), its average is 0.29, which partitions the 10 numbers into two groups: those greater than the average (1, 1/2, 1/3) called the head, and those less than the average (1/4, 1/5, 1/6, ... 1/10) called the tail. For those in the head (1, 1/2, 1/3), their average is 0.61, which further partitions the three into two groups: the one greater than the average (1) called the head and those less the average (1/2, 1/3) called the tail. The number of iterations or the notion of far more smalls than larges occurs twice, so the ht-index is three, indicating three inherent hierarchical levels. As shown in this example, the head percentage is far less than the preset 40%. The 40% is a very loose condition for something to be a minority to meet the notion far more smalls than larges.

In this study, we detect power laws using the robust maximum likelihood method (Clauset et al. 2009), calculate the ht-index for all COVID-19 cases in the US, and compare these calculated parameters with those of the population at both state and county levels along the time dimension. This type of comparison provides new insights into the spatiotemporal patterns of the pandemic. Before getting into the results, we would like to make one point explicitly clear about power law exponent  $a$ . It is a good indicator for heterogeneity of data: the higher the exponent, the more heterogeneous the data. For example, given two power laws,  $y = x^{-2}$ , and  $y = x^{-3}$ , the one with the exponent 3 is more heterogeneous than the one with the exponent 2. Throughout our study, we will show that the ht-index is a better indicator than the power law exponent for characterizing the data heterogeneity.

## Results and discussion

The population of the US looks like a power law distribution at both state and

county levels, as shown in Figure 2, but they are power laws with an exponential cut-off, strictly speaking. It is pretty

the same for both infection and death gradually developing towards power laws with cut-off as time passes (shown as

**Table 1: Support of a moderate power law or a power law with cut-off in comparison to alternatives**

(Note: LR = likelihood ratio, PL = power law,  $p$  = p-value as defined in Clauset et al. 2009)

	Lognormal		Exponential		PL with cutoff		Support
	LR	P	LR	P	LR	$p$	
Week 12	-4.74	0.1	122.24	0.02	-4.46	0	moderate PL
Week 13	-0.29	0.82	229.23	0.03	-0.2	0.52	moderate PL
Week 14	-0.03	0.9	182.22	0.03	-0.02	0.86	moderate PL
Week 15	-0.3	0.68	175.6	0.03	-0.18	0.55	moderate PL
Week 16	-4.04	0.01	514.44	0	-2.35	0.03	PL with cutoff
Week 17	-1.68	0.27	340.5	0	-1.62	0.07	PL with cutoff
Week 18	-1.51	0.29	353.76	0	-1.6	0.07	PL with cutoff
...							
Week 27	-2.21	0.18	308.44	0	-3.48	0.01	PL with cutoff
Week 28	-2.66	0.14	328.65	0	-3.78	0.01	PL with cutoff

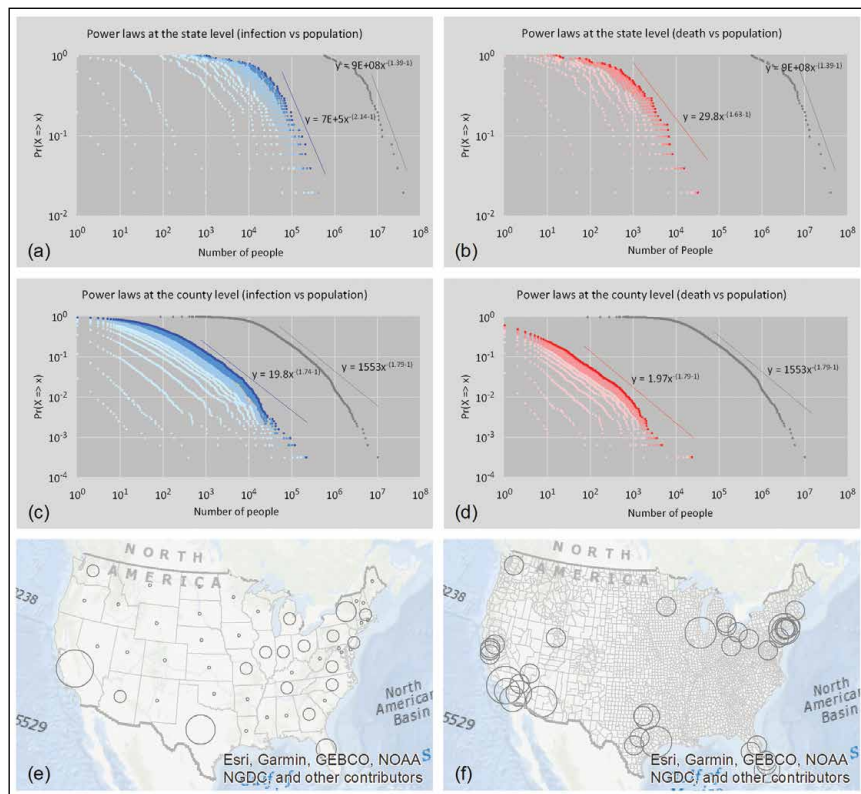


**Figure 2: (Color online) Power laws of infection (blue), death (red), and population (gray)** (Note: At the state level (a, b), because of the large areal unit, the power laws with cut-off are not so striking, whereas at the county level (c, d), because of the small areal unit, the power law with cut-off are very striking. The hierarchy of population is mapped both (e) state and (f) county levels, indicating far more less-populated states than well-populated ones, or far more less-populated counties than well-populated ones. Interestingly, the notion of far more smalls than large recurs four and six times at the state and county levels, respectively, thus with the ht-indexes being 5 and 7, indicating the inherent hierarchical levels. All the five levels are shown in panel (e), whereas only the top four levels are shown in panel (f) for the sake of legibility.)

light blue and light red to dark blue and dark red). In March or before early April, both infection and death exhibit moderate power laws, while after April they are power laws with cut-off. As an example, Table 1 shows that how death at the county level demonstrate a power law or a power law with cut-off with detailed statistics.

The likelihood ratio (LR) (Clauset et al. 2009) can be used to determine power laws or power laws with cut-off hold in comparison to its alternative heavy tailed distributions such as lognormal and exponential. As a rule, a positive LR favors the power law fit, while a negative LR says the alternative fit. On the other hand, the LR is trustworthy if the statistical fluctuation of LR is relatively small. Therefore, an additional p-value is defined to the LR is trustworthy statistically (Clauset et al., 2009); if  $p < 0.1$ , then the LR is trustworthy.

At the state level, the LR is not statistically significant as the p-values are too high, therefore we cannot be certain that either of the distributions is a better fit. This is likely due to the small sample size ( $n = 51$ ). At the county level with the large sample ( $n = 3262$ ), the alternative lognormal distribution is more likely than the power law distribution for most of the weeks. However, the support for power laws with cut-off are even more likely than the lognormal distribution. In the end, power laws with cut-off are more likely than the lognormal and exponential distributions.

The log-log plots in Figure 2 indicate that the overall spatial distributions of infection and death are very much shaped by the underlying population. That is, those populated states and counties tend to have far more cases of infection or death. This is of course not out of our expectation, since the more the population, the more likely the infection or death. Given the power law distribution of the population and by applying the head/tail breaks, we derive ht-indexes of 5 and 7 at the state and county levels, respectively. In other words, the population is automatically classified into 5 and 7 classes, as shown

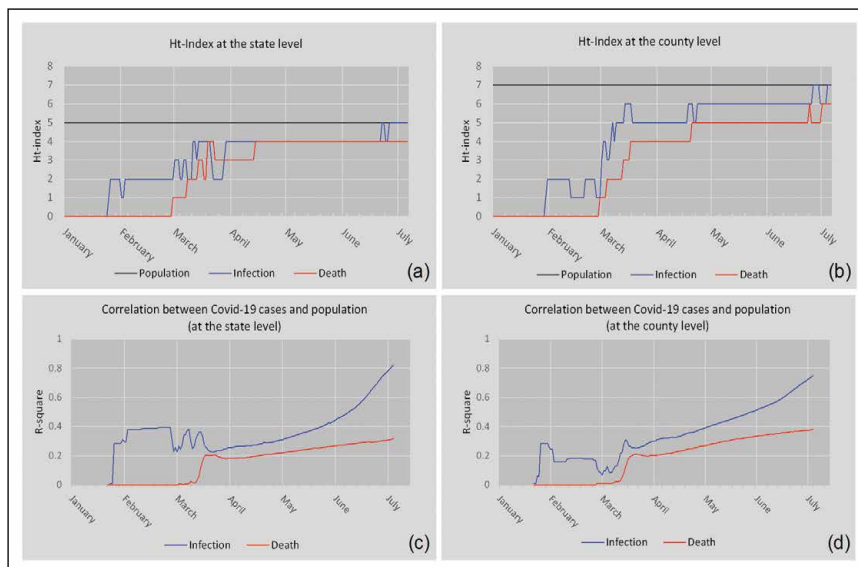


**Figure 3: (Color online) Relationship between COVID-19 cases and populations** (Note: The ht-indexes for the population are 5 and 7 respectively at the state (a) and county (b) levels, while the ht-indexes for the infection and death increase from mild to wild status despite some slight fluctuations. The correlations between infection and population, and between death and population increase at both the state (c) and county (d) levels.)



**Figure 4: (Color online) The hierarchy of COVID-19 cases compared with that of population** (Note: Each state has three circles: gray for population, blue for infection, and red for death. Panels (a)–(f) show the status of the pandemic in January, February, March, April, May, and June respectively at the state level. For the county level, please refer to the animation map at <http://lifegis.hig.se/COVID19/>.)

in Figure 2 (e, f). These two patterns regarding population at the state and county levels reflect the patterns of COVID-19 cases fairly well. That is, the states and counties on the West and East Coasts tend to have higher numbers of COVID-19 cases than those inland, which will be examined in the following. These two patterns at the state and county levels constitute the basic patterns to which COVID-19 cases can be compared in order to develop new insights into the pandemic in terms of its spatial and temporal patterns.

It is clear from Figure 2 that the power law distributions have different exponents. The different power law exponents indicate the different degree of heterogeneity or hierarchy; that is, the higher the exponents, the more heterogeneous the data. In this connection, the ht-index is a better indicator than the power exponent as it better reflects the inherent hierarchy. As shown in Figure 3a and 3b, the ht-indexes of both infection and death increase towards that of population. There is little wonder that the ht-index of the population remains unchanged – that is, 5 at the state level and 7 at the county level – indicating that the population is more heterogeneous at the county level than that in the state level (Figure 3a and 3b). This is because the population in the large areal unit of states tends to be more homogenized than that in the small areal unit of counties. According to this logic, the population in the small areal unit of cities tends to be more heterogenized than that in the large areal unit of counties. This is indeed true, as shown in the literature (e.g., Newman 2005). What is interesting for infection and death is that they have a very low ht-index of 0 or 1 at the very beginning and increase rapidly towards 5 and 7, with some fluctuation in the course of development of the pandemic. This means that lockdown policies or social distancing measures are definitely effective at containing and combating the spread of the virus; otherwise, the situation would be far more devastating than it is currently. The result shows that

COVID-19 cases are largely shaped by the underlying population, seen through the increasing correlations between infection and population and between death and population (Figure 3c and 3d). In other words, two patterns shown in Figure 2 (e, f) largely reflect those of infection and death; that is, populated states and counties tend to have far more COVID-19 cases.

As elaborated above, the ht-indexes of infection and death at both the state and country levels are persistently approaching to that of population, and the correlations between infection and population, and between death and population increase also as time goes (Figure 3). This is the overall picture. On the other hand, the hierarchical levels for these three parameters (population, infection, and death) provide a much more complex and interesting picture about the pandemic (Figure 4). By examining the ht-indexes of the three parameters (population, infection and death) for individual states and counties, we can see how the pandemic hits individual states and counties differently relative to their total populations. For example, New York and its nearby states are hit most hard as reflected by the larger red circles, whereas California and Texas are affected far less, as shown by larger gray circles (Figure 4d). It is important to assess how this latest situation evolved from a dynamic point of view. For example, the situation in January and February was very mild; only five states had a relatively high degree of infection, with Washington State having the highest. The situation took a drastic turn into very wild in March, when there were suddenly six states with larger red circles, indicating that hierarchical levels of death were larger than those of population and infection. This was a dangerous sign. From March to April, and from May to June, the situation got worsened, with a few exceptions such as Washington State. These are the new insights that are developed from the state level. The same insights can be seen at the county level, and the reader can refer to or further explore the animation map as cited in the note of Figure 4.

## Implication

This study has an important implication for power-law-related studies. The distributions of many natural and societal phenomena follow a power law over a wide range of magnitude, which has been extensively studied in a variety of scientific fields, such as physics, biology, economics, geography, demography, and social sciences (e.g., Bak 1996, Newman 2005). Surrounding a power law distribution and its variants such as lognormal and exponential, an increasing number of research works have been made to illustrate what is the appropriate distribution for a real-world data. The first author of this paper has long developed an argument that a power law is an idealist status, when a complex system becomes mature or well-developed (Jiang and Yin 2014). Before the idealized status, the system is likely to show some deviation from a power law, thus a less-power-law distribution such as lognormal or a power law with an exponential cutoff. In this regard, it is better to use the ht-index to characterize the dynamic process or evolution of the system. This study proves that the ht-index is a good indicator, apparently a better one than the power law exponent, for characterizing the inherent hierarchy or heterogeneity of a complex system from a dynamic point of view.

## Conclusion

In this paper, we have found that COVID-19 cases in the United States have developed over time from a less heterogeneous state to a more heterogeneous one, or equivalently from a very flat hierarchy to a very steep hierarchy, persistently approaching that status of the populations. Thus, the COVID-19 spatiotemporal patterns are largely shaped by the underlying population patterns, i.e., well-populated states or counties tend to have more people affected or died. While this finding may seem obvious, deviations from this overall trend help us see the particularities of the COVID-19 patterns at local scales. On the one hand, the spatial distribution

of COVID-19 cases is persistently approaching a power law with cut-off, despite the implemented lockdown and social distance measures, indicating enormous spatial heterogeneity in terms of the distribution of COVID-19 cases. On the other hand, the observation that the ht-index of COVID-19 cases does not exceed that of population implies that lockdown and social distance measures do indeed have some effect; otherwise, the situation would become far more devastating than it is now. The power-law-based approach enables us to uncover these interesting patterns of COVID-19 cases, so opens a new way of mapping geographic phenomena. Our future work points to this direction.

## Data availability statement

The data used and generated in this study are available at <https://doi.org/10.6084/m9.figshare.13295540>. The covid-19 data is based on the GitHub repository maintained by Johns Hopkins University (2020). It can be found at: [https://github.com/CSSEGISandData/COVID-19/tree/master/csse\\_covid\\_19\\_data](https://github.com/CSSEGISandData/COVID-19/tree/master/csse_covid_19_data). Powerlaw calculations have been done with Aaron Clauset's MatLab code found at: <http://tuvalu.santafe.edu/~aaronc/powerlaws/>. The software used to spatially process and visualize the data is ArcGIS 10.7 by ESRI. Additionally head/tail breaks have been calculated with a head/tail breaks calculator which can be found at: <https://github.com/ChrisdeRijke/HeadTailBreaksCalculator>

## Notes on contributors

Dr. Bin Jiang (ORCID: 0000-0002-2337-2486) is professor of computational geography at Faculty of Engineering and Sustainable Development (Division of GIScience) of the University of Gävle, Sweden. His research interests center on geospatial analysis of urban structure and dynamics, e.g., topological analysis, and scaling hierarchy applied to buildings, streets, and cities, or geospatial big data in general. Inspired

by Christopher Alexander's work, he developed a mathematical model of beauty - beautimeter, which helps address not only why a structure is beautiful, but also how much beauty the structure is.

Mr. Chris de Rijke (ORCID: 0000-0003-4739-7781) is a research assistant at Faculty of Engineering and Sustainable Development (Division of GIScience) of the University of Gävle, Sweden. He holds bachelor and master's degrees in earth sciences and economics, and recently a master's degree in GIS. He has been researching on living structure and topological analysis supported by the novel concepts of natural cities and natural streets using big data such as OpenStreetMap data, nighttime imagery, and social media data.

## Acknowledgement

This paper is reprinted from the open-access paper (Jiang and de Rijke 2021) with permission of the publisher Taylor & Francis. We would like to thank the anonymous referees for their valuable comments and Dr. Aaron Clauset for his insightful discussion. This paper was partially supported by the Swedish Research Council FORMAS through the ALEXANDER project with grant number FR-2017/0009.

## References

- Bak P. (1996), *How Nature Works: the Science of Self-organized Criticality*, Springer-Verlag: New York.
- Clauset A., Shalizi C. R., and Newman M. E. J. (2009), Power-law distributions in empirical data, *SIAM Review*, 51, 661-703.
- ESRI (2020), *COVID-19 GIS Hub*, <https://coronavirus-disasterresponse.hub.arcgis.com/>  
[https://github.com/CSSEGISandData/COVID-19/tree/master/csse\\_covid\\_19\\_data](https://github.com/CSSEGISandData/COVID-19/tree/master/csse_covid_19_data)
- Jiang B. (2013), Head/tail breaks: A new classification scheme for data with a

heavy-tailed distribution, *The Professional Geographer*, 65 (3), 482-494.

Jiang B. (2015), Geospatial analysis requires a different way of thinking: The problem of spatial heterogeneity, *GeoJournal*, 80(1), 1-13. Reprinted in Behnisch M. and Meinel G. (editors, 2017), *Trends in Spatial Analysis and Modelling: Decision-Support and Planning Strategies*, Springer: Berlin, 23-40.

Jiang B. and de Rijke C. (2021), A power-law-based approach to mapping COVID-19 cases in the United States, *Geo-spatial Information Science*, x(x), xx-xx. <https://doi.org/10.1080/10095020.2020.1871306>

Jiang B. and Slocum T. (2020), A map is a living structure with the recurring notion of far more smalls than larges, *ISPRS International Journal of Geo-Information*, 9(6), 388, <https://www.mdpi.com/2220-9964/9/6/388>, Reprinted as the cover story in the magazine *Coordinates*, August issue, 6-17, 2020.

Jiang B. and Yin J. (2014), Ht-index for quantifying the fractal or scaling structure of geographic features, *Annals of the Association of American Geographers*, 104(3), 530-541.

Johns Hopkins University (2020), *COVID-19 Data Repository by the Center for Systems Science and Engineering (CSSE) at Johns Hopkins University*,

Koch R. (1998), *The 80/20 Principle: The secret of achieving more with less*, DOUBLEDAY: New York.

Newman M. E. J. (2005), Power laws, Pareto distributions and Zipf's law, *Contemporary Physics*, 46(5), 323-351.

Surowiecki J. (2004), *The Wisdom of Crowds: Why the Many Are Smarter than the Few*, ABACUS: London.

Zipf G. K. (1949), *Human Behavior and the Principles of Least Effort*, Addison Wesley, Cambridge, MA. ▽

# Coverage and optimal visibility-based navigation using visibility analysis from geospatial data

In this paper, we study the multi-sensors placement optimization problem in 3D urban environments for optimized coverage



**Oren Gal**  
Mapping and Geo-  
information, Technion,  
I.I.T., Israel



**Yerach Doytsher**  
Mapping and Geo-  
information, Technion,  
I.I.T., Israel

**M**odern cities and urban environments are becoming denser more heavily populated and are still rapidly growing, including new infrastructures, markets, banks, transportation, etc.

In the last two decades, more and more cities and mega-cities have started using multi-camera networks in order to face this challenge. However, this is still not enough. Multi-sensor placement in 3D urban environments is not a simple task, also known as NP-hard one.

In this paper, we study the multi-sensors placement optimization problem in 3D urban environments for optimized coverage. The first part of our research presents a unique solution for the 3D visibility problem in built-up areas. In the second part, we present optimized coverage using multi-sensors in 3D model based on genetic algorithms using novel visibility analysis. The solutions presented in this paper can be used, among other algorithms and solutions, to enable optimal coverage and moreover optimal trajectory planning and navigation based on an optimal visibility points.

## Introduction and related work

Modern cities and urban environments are becoming denser and more heavily populated and are still rapidly growing, including new infrastructures, markets, banks, transportation etc.

At the same time, security needs are becoming more and more demanding

in our present era, in the face of terror attacks, crimes, and the need for improving law enforcement capabilities, as part of the increasing global social demand for efficient and immediate homeland and personal security in modern cities.

In the last two decades, more and more cities and mega-cities have started using multi-camera networks in order to face this challenge, mounting cameras for security monitoring needs [1]; however, this is still not enough [30]. Due to the complexity of working with 3D and the dynamic constraints of urban terrain, sensors were placed in busy and populated viewpoints, to observe the occurrences at these major points of interest.

These current multi-sensors placement solutions ignore some key factors, such as: visibility analysis in 3D models, which also consist of unique objects such as trees; changing the visibility analysis aspect from visible or invisible states to semi-visible cases, such as trees, and above all, optimization solutions which take these factors into account.

Multi-sensor placement in 3D urban environments is not a simple task. The optimization problem of the optimal configuration of multi sensors for maximal coverage is a well-known Non-deterministic Polynomial-time hard (NP-hard) one [5], even without considering the added complexity of urban environments.

An extensive theoretical research effort has been made over the last four decades, addressing a much simpler problem in 2D known as the art gallery problem, with unrealistic assumptions such as unlimited visibility for each agent, while the 3D problem has not received special attention [8][28][35].

The coupling between sensors' performances and their environment's constraints is, in general, a complex optimization problem. In this paper, we study the multi-sensors placement optimization problem in 3D urban environments for optimized coverage based on genetic algorithms using novel visibility analysis.

Our optimization solution for this problem relates to maximal coverage from a number of viewpoints, where each 3D position (x, y, z coordinates) of the viewpoint is set as part of the optimized solution. The search space contains local minima and is highly non-linear. The Genetic Algorithms are global search methods, which are well-suited for such tasks. The optimization process is based on randomly generating an initial population of possible solutions (called chromosomes) and, by improving these solutions over a series of generations, it is able to achieve an optimal solution [36].

Multi-sensor placements are scene- and application- dependent, and for this reason generic rules are not very efficient at meeting these challenges. Our approach is based on a flexible and efficient analysis that can handle this complexity.

The total number of sensors is a crucial parameter, due to the real-time outcome data that should be monitored and tracked, where too many sensors are not an efficient solution. We address the sensor numbers that should be set as a tradeoff of coverage area and logical data sources that can be monitored and tracked.

As part of our high-dimension optimization problem, we present several 3D models, such as B-ref, sweeping and wireframe models, Polyhedral Terrain

Models (PTM) and Constructive Solid Geometry (CSG) for an efficient 3D visibility analysis method, integrating trees as part of our fast and efficient visibility computation, thus extending our previous work [25] to 3D visible volumes.

Accurate visibility computation in a 3D environments is a very complicated process demanding a high computational effort, which cannot be easily carried out in a very short time using traditional well-known visibility methods [41]. The exact visibility methods are highly complex, and cannot be used for fast applications due to their long computation time. As mentioned above, previous research in visibility computation has been devoted to open environments using Digital Elevation Model (DEM) models, representing raster data in 2.5D (Polyhedral model), which do not address, or suggest solutions for, densely built-up areas.

One of the most efficient methods for DEM visibility computation is based on shadow-casting routine. The routine casts shadowed volumes in the DEM, like a light bubble [42]. Other methods related to urban design environment and open space impact treat abstract visibility analysis in urban environments using DEM, focusing on local areas and approximate openness [20]. Extensive research treated Digital Terrain Models (DTM) in open terrains, mainly Triangulated Irregular Network (TIN) and Regular Square Grid (RSG) structures. Visibility analysis on terrain was classified into point, line and region visibility, and several algorithms were introduced based on horizon computation describing visibility boundaries [11] [12].

A vast number of algorithms have been suggested for speeding up the process and reducing computation time [38]. Franklin [21] evaluates and approximates visibility for each cell in a DEM model based on greedy algorithms. An application for siting multiple observers on terrain for optimal visibility cover was introduced in [23]. Wang et al. [52] introduced a Grid-based DEM method using viewshed horizon, saving computation time based on relations between surfaces and Line

Of Sight (LOS), using a similar concept of Dead-Zones visibility [4]. Later on, an extended method for viewshed computation was presented, using reference planes rather than sightlines [53].

Most of these published papers have focused on approximate visibility computation, enabling fast results using interpolations of visibility values between points, calculating point visibility with the Line of Sight (LOS) method [13]. Other fast algorithms are based on the conservative Potentially Visible Set (PVS) [16]. These methods are not always completely accurate, as they may render hidden objects' parts as visible due to various simplifications and heuristics.

Only a few works have treated visibility analysis in urban environments. A mathematical model of an urban scene, calculating probabilistic visibility for a given object from a specific viewcell in the scene, has been presented by [37]. This is a very interesting concept, which extends the traditional deterministic visibility concept. Nevertheless, the buildings are modeled as cylinders, and the main challenges of spatial analysis and model building were not tackled. Other methods have been developed, subject to computer graphics and fields of vision, dealing with exact visibility in 3D scenes, without considering environmental constraints. Concerning this issue, Plantinga and Dyer [41] used the aspect graph – a graph with all the different views of an object. Shadow boundaries computation is a very popular method, studied by [14][47][48]. All of these works are not applicable to a large scene, due to computational complexity.

As mentioned, online visibility analysis is a very complicated task. Recently, off-line visibility analysis, based on preprocessing, was introduced. Cohen-Or et al. [4] used a ray-shooting sample to identify occluded parts. Schaufler et al. [44] use blocker extensions to handle occlusion.

Since visibility analysis in 3D urban environments is a very complicated task, it is therefore our main optimization

function, known as Fitness. We introduce an extended visibility aspect for the common method of Boolean visibility values, “1” for objects seen and “0” for objects unseen from a specific viewpoint, and treat trees as semi-visibility values (such as partially seen, “0.5” value), thereby including in our analysis the real environmental phenomena which are commonly omitted.

We extend our previous work and propose fast and exact 3D visible volumes analysis in urban scenes based on an analytic solution, integrating trees into our 3D model, and it is demonstrated with a real urban scene model from Neve-Sha’anan neighborhood (within the city of Haifa).

In the following sections, we first introduce an overview of 3D models and our demands from these models. In the next section, we extended the 3D visible volumes analysis which, for the first time, takes trees into account. Later on, we present the simulation using the Neve-Sha’anan neighborhood (within the city of Haifa) 3D model. We present our genetic algorithm optimization stages and simulation based on our 3D visible volumes analysis, taking trees into account. Eventually, we extend our current visibility aspect and include conditions necessary for visibility based on the sensor’s stochastic character and present the effect of these limitations on our visibility analysis.

### Analytic 3D visible volumes analysis

In this section, we present fast 3D visible volumes analysis in urban environments, based on an analytic solution which plays a major role in our proposed method of estimating the number of clusters. We briefly present our analysis presented in [27], extending our previous work [25] for surfaces’ visibility analysis, and present an efficient solution for visible volumes analysis in 3D.

We analyze each building, computing visible surfaces and defining visible pyramids using analytic computation for visibility boundaries [25]. For each object we define Visible Boundary Points (VBP) and Visible Pyramid (VP).

A simple case demonstrating an analytic solution from a visibility point to a building can be seen in Figure 5(a). The visibility point is marked in black, the visible parts colored in red, and the invisible parts colored in blue where VBP are marked with yellow circles.

In this section, we briefly introduce our concept for visible volumes inside bounding volume by decreasing visible pyramids and projected pyramids to the bounding volume boundary. First, we define the relevant pyramids and volumes.

**The Visible Pyramid (VP):** we define  $VP_i^{j=1..N_{surf}}(x_0, y_0, z_0)$  of object  $i$  as a 3D pyramid generated by connecting VBP of specific surface  $j$  to a viewpoint  $V(x_0, y_0, z_0)$ .

In the case of a box, the maximum number of  $N_{surf}$  for a single object is three. VP boundary, colored with green arrows, can be seen in Figure 5(b).

For each VP, we calculate Projected Visible Pyramid (PVP), projecting VBP to the boundaries of the bounding volume  $S$ .

**Projected Visible Pyramid (PVP)** - we define  $PVP_i^{j=1..N_{surf}}(x_0, y_0, z_0)$  of object  $i$  as 3D projected points to the bounding volume  $S$ , VBP of specific surface  $j$  through viewpoint  $V(x_0, y_0, z_0)$ . VVP boundary, colored with purple arrows, can be seen in Figure 6.

The 3D Visible Volumes inside bounding volume  $S$ , VVs, computed as the total bounding volume  $S$ , Vs minus the Invisible Volumes IVs. In a case of no overlap between buildings,

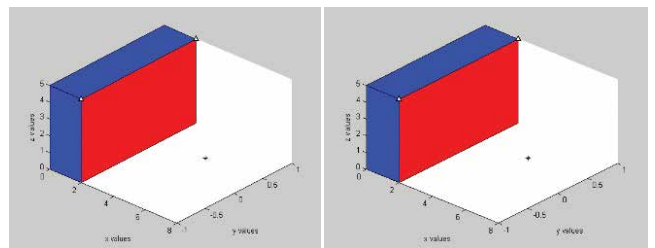


Figure 1: (a) Visibility Volume Computed with the Analytic Solution. (b) Visible Pyramid from a Viewpoint (marked as a Black Dot) to VBP of a Specific Surface (source: [27]).

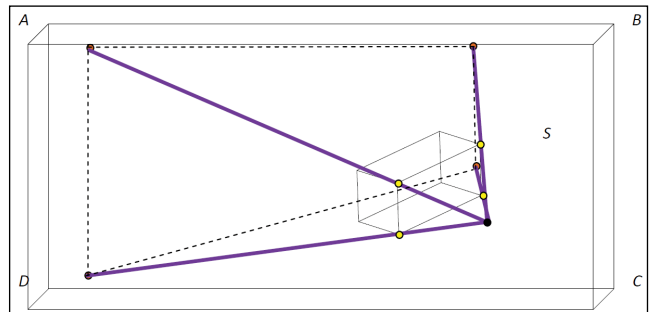


Figure 2: Invisible Projected Visible Pyramid Boundaries colored with purple arrows from a Viewpoint (marked as a Black Dot) to the boundary surface ABCD of Bounding Volume  $S$  (source: [27]).

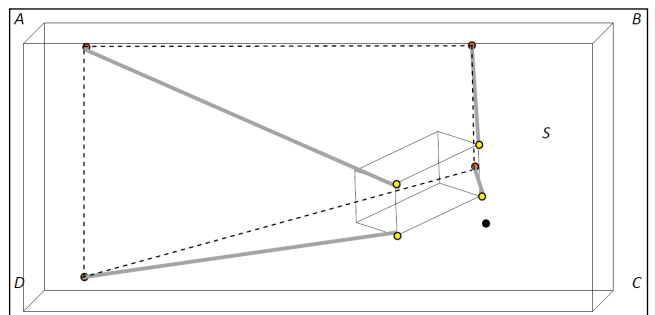


Figure 3: Invisible Volume Colored in Gray Arrows. Decreasing Projected Visible Pyramid boundary surface ABCD of Bounding Volume  $S$  from Visible Pyramid (source: [27]).

IVs is computed by decreasing the visible volume from the projected visible volume,  $\sum_{i=1}^{N_{obj}} \sum_{j=1}^{N_{surf}} (V(PVP_i^j) - V(VP_i^j))$ .

$$VV_S = V_S - \sum_{i=1}^{N_{obj}} \sum_{j=1}^{N_{surf}} IV_{S_i}^j$$

$$VV_S = V_S - \sum_{i=1}^{N_{obj}} \sum_{j=1}^{N_{surf}} (V(PVP_i^j) - V(VP_i^j))$$

By decreasing the invisible volumes from the total bounding volume, only the visible volumes are computed, as seen in Figure 7. Volumes of PVP and VP can be simply computed based on a simple pyramid volume geometric formula.

**Invisible Hidden Volume (IHV)** - We define Invisible Hidden Volume (*IHV*), as the *Invisible Surface (IS)* between visible pyramids projected to bounding box *S*.

The *PVP* of the object close to the viewpoint is marked in black, colored with pink circles denoted as boundary set points  $\{B_{11}, \dots, B_{18}\}$  and the far object's *PVP* is colored with orange circles, denoted as boundary set points  $\{C_{11}, \dots, C_{18}\}$ . It can be seen that *IHV* is included in each of these invisible volumes, where  $\{A_{11}, \dots, A_{18}\} \in \{B_{11}, \dots, B_{18}\}$  and  $\{A_{11}, \dots, A_{18}\} \in \{C_{11}, \dots, C_{18}\}$  and, as can be seen in Figure 8.

Therefore, we add *IHV* between each overlapping pair of objects to the total visible volume. In the case of overlapping between objects' visible pyramids, 3D visible volume is formulated as:

$$VV_S = V_S - \sum_{i=1}^{N_{obj}} \sum_{j=1}^{N_{surf}} (V(PVP_i^j) - V(VP_i^j) + IHV_i^j) \quad (2)$$

The same analysis holds true for multiple overlapping objects, adding the *IHV* between each two consecutive objects.

Extended formulation for two buildings with or without overlap can be seen in [27].

### Partial Visibility Concept - Trees

In this research, we analyze trees as constant objects in the scene, and formulate a partial visibility concept. In our previous work, we tested trees as dynamic objects and their effect on visibility analysis [26]. Still, the analysis focused on trees' branches over time, setting visible and invisible values for each state, taking into account probabilistic modeling in time.

We model trees as two boxes [40], as seen in Figure 9. The lower box, bounded between  $[0, h_1]$  models the tree's trunk, leads to invisible volume and is analyzed as presented previously, for a box modeling building's structures. On the other hand, the upper box bounded between  $[h_1, h_2]$  is defined as partially visible, since a tree's leaves and the wind's effect are hard to predict and continuously change over time. Due to these inaccuracies, we set the projected surfaces and the Projected Visible Pyramid of this box as half visible volume.

According to that, a tree's effect on our visibility analysis is divided into regular boxes included in the total number of objects,  $N_{obj}$  (identical to the building case), and the upper boxes modeling the tree's leaves, denoted as  $N_{trees}$ . The total 3D visible volumes can be formulated as:

$$VV_S = V_S - \sum_{i=1}^{N_{obj}} \sum_{j=1}^{N_{surf}} (V(PVP_i^j) - V(VP_i^j) + IHV_i^j) - \sum_{i=1}^{N_{trees}} \sum_{j=1}^{N_{surf}} \frac{1}{2} (V(PVP_i^j) - V(VP_i^j) + IHV_i^j) \quad (3)$$

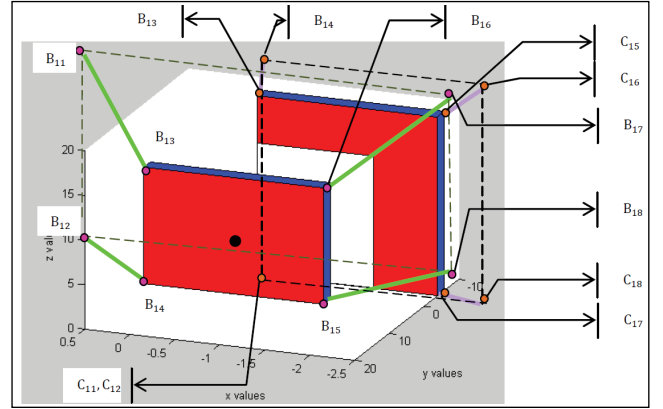


Figure 4: Invisible Volume colored in purple and green arrows for each building. PVP of the object close to viewpoint colored in black, colored with pink circles and the far object PVP colored with orange circle (source: [27]).

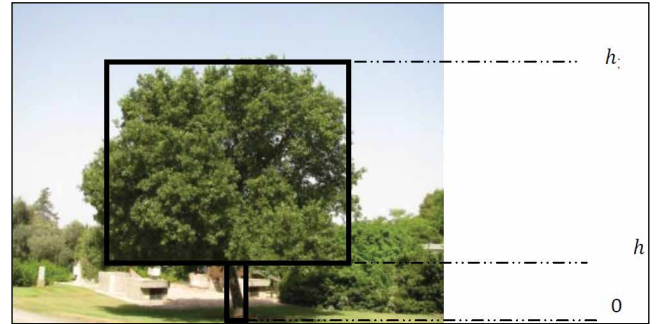


Figure 5: Modeling a Tree Using Two Bounding Boxes.



Figure 6: Views of Neve-Sha'an Street, Haifa, Israel from Google Maps source: [20]

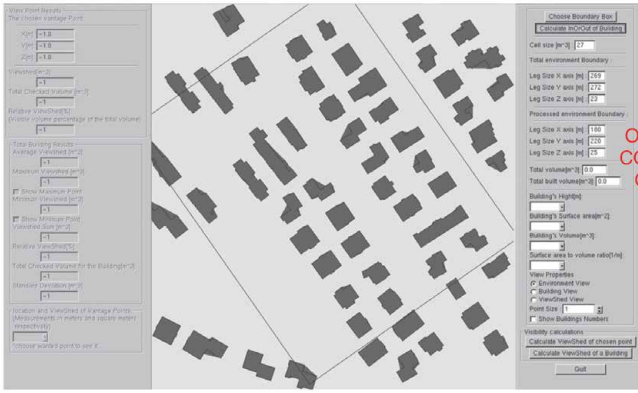


Figure 7: AutoCAD model of Neve-Sha'an Street, Haifa, Israel.

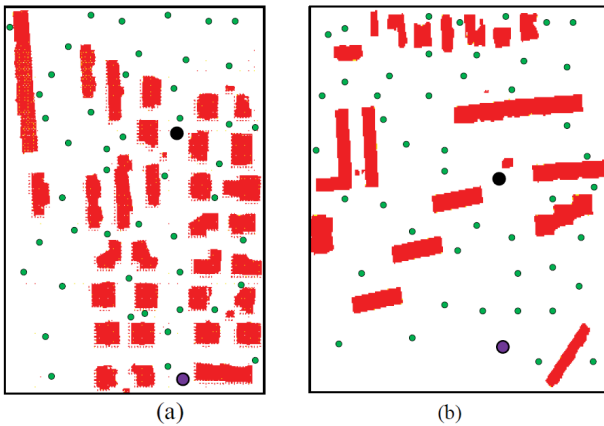


Figure 8: Tested Scenes with Trees marked with green points, Viewpoint 1 Colored in Black, Viewpoint 2 Colored in Purple : (a) Small-scale housing in dense environments; (b) Multi-story buildings in an open area.

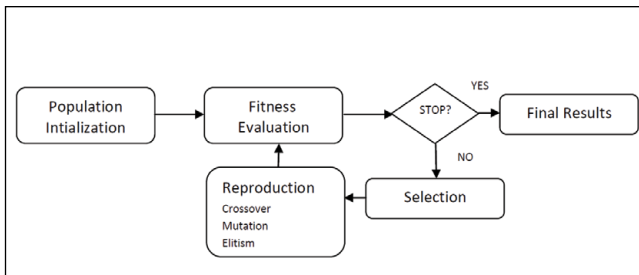


Figure 9: GA Block Diagram, source: [31].

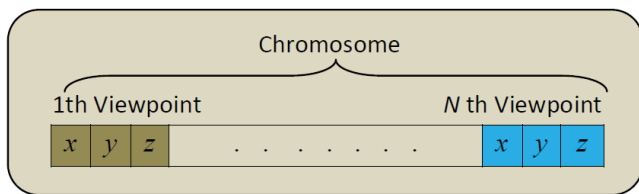


Figure 10: An individual in the GA search is also called "Chromosome". In our case it represents one possible sensor's location for N viewpoints computing 3D visible volumes analysis with trees.

## Simulations

In this section, we demonstrate our 3D visible volumes analysis in urban scenes integrated with trees, presented in the previous section. We have implemented the presented algorithm and tested some urban environments on a 1.8GHz Intel Core CPU with Matlab. Neve-Sha'an Street in the city of Haifa was chosen as a case study, presented in Figure 10.

We modeled the urban environment into structures using AutoCAD model, as seen in Figure 11, with bounding box S. By using the Matlab©MathWorks software, we automated the transformation of data from AutoCAD structure to our model's internal data structure.

Our simulations focused on two cases: (1) small-scale housing in dense environments; (2) Multi-story buildings in an open area. These two different cases do not take the same objects into account. The first viewpoint is marked with black dot and the second one marked in purple, as seen in Figure 12. Since trees are not a part of our urban scene model, trees are simulated based on similar urban terrain in Neve-Sha'an. We simulated fifty trees' locations using standard Gauss normal distribution, where the trees' parameters are defined randomly  $h_1 \in (0.3, 0.9)$ ,  $h_2 \in (1.5, 3)$ , as seen in Figure 12.

We set two different viewpoints, and calculated the visible volumes based on our analysis presented in the previous sub-section. Visible volumes with time computation for different cases of bounding boxes' test scenes are presented in Table II and Table III.

One can notice that the visible volumes become smaller in the dense environments described in Table II, as we enlarge the bounding box. Since we take into account more buildings and trees, less volumes are visible and the total visible volumes from the same viewpoint are smaller.

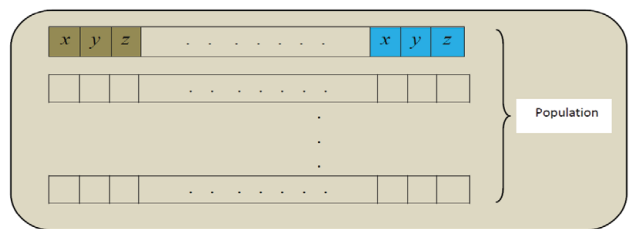


Figure 11: Population of GA search with N chromosomes.

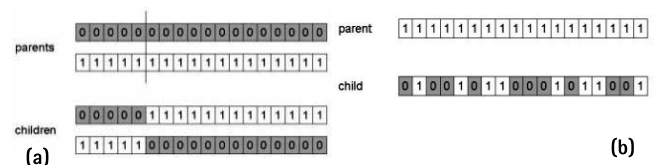


Figure 12: Reproduction operators of GA (a) Crossover (b) Mutation source: [17].

### Visible Volumes and Computation Time for Small-Scale Housing Case

Bounding Box	Viewpoint	Visible Volumes [10 <sup>6</sup> .m <sup>3</sup> ]	Computation Time [sec]
[100 m *100 m * 100 m]	Viewpoint 1	321.7	19.6
	Viewpoint 2	486.8	
[200 m * 200 m * 200 m]	Viewpoint 1	547.4	20.8
	Viewpoint 2	584.2	

### Visible Volumes for Small Multi-story Buildings Case

Bounding Box [100 m *100 m * 100 m]	Visible Volumes [10 <sup>6</sup> .m <sup>3</sup> ]	Computation Time [sec]
Viewpoint 1	3453	22.9
Viewpoint 2	3528	

### 3D Visible Volumes – Pseudo Code

Given viewpoint  $V(x_0, y_0, z_0)$

1. Calculate bounding volume  $V_S$

2. For  $i=1:N_{obj}$  building models

2.1. Calculate Azimuth  $\theta_i$  and Distance  $D_i$  from viewpoint to object

2.2. Set and Sort Buildings Azimuth Array  $\theta[i]$

2.3. IF Azimuth Objects ( $i, 1..i-1$ ) Intersect

2.3.1. Sort Intersected Objects  $j=1:N_{intersect}$  by Distance

2.3.2. Compute VBP for each intersected building,  $VBP_{j=1..N_{intersect}}^{1..N_{bound}}$

2.3.3. Generate VP for each intersected building,  $VP_{j=1..N_{intersect}}^{1..N_{obj}}$

2.3.4. Set  $PVP_i^j$  and  $IHV_i^j$  volumes for objects,  $N_{obj}$

2.3.5. Set  $PVP_i^j$  and  $IHV_i^j$  volumes for Trees,  $N_{Trees}$

Else

2.3.6. Compute VBP for each object,  $VBP_{j=1..N_{intersect}}^{1..N_{bound}}$

2.3.7. Generate VP for each building,  $VP_{j=1..N_{intersect}}^{1..N_{obj}}$

2.3.8. Set  $PVP_i^j$  volumes for objects,  $N_{obj}$

2.3.9. Set  $PVP_i^j$  volumes for Trees,  $N_{Trees}$

End

2.4. Calculate Visible Volumes  $VV_S$

End

### Complexity analysis

We analyze our algorithm complexity based on the pseudo code presented in the previous section, where  $n$  represents the number of buildings and trees. In the worst case,  $n$  objects hide each other. Visibility complexity consists of generating VBP and VPV for  $n$  objects,  $nO(1)$  complexity. Projection and intersection are also  $nO(1)$  complexity. The complexity of our algorithm, without considering data structure managing for urban environments, is .

### Optimized coverage using genetic algorithms

The Genetic Algorithm (GA) presented by Holland [31] is one of the most common algorithms from the evolutionary algorithms class used for complex optimization problems in different fields, such as: pharmaceutical design [33], financial forecasting [50], tracking and coverage [18][39][45], and bridge design [24]. These kinds of algorithms, inspired by natural selection and genetics, are sometimes criticized for their lack of theoretical background due to the fact that in some cases the outcome is unpredictable or difficult to verify.

The main idea behind GA is based on repeated evaluation of individuals (which are part of a candidate solution) using an objective function over a series of generations. These series are improved over generations in order to achieve an optimal solution. In the next paragraphs, we present the genetic algorithms' main stages, adapted to our specific problem.

The major stages in the GA process (evaluation, selection, and reproduction) are repeated either for a fixed number of generations, or until no further improvement is noted.

The common range is about 50-200 generations, where fitness function values improve monotonically [31].

A block diagram of GA is depicted in Figure 13.

**Population initialization:** The initialization stage creates the first generation of candidate solutions, also called chromosomes. A population of candidate solutions is generated by a random possible solution from the solution space. The number of individuals in the population is dependent on the size of the problem and also on computational capabilities and limitations. In our case it is defined as 500 chromosomes, due to the fact that 3D visible volumes must be computed for each candidate.

---

The exact visibility methods are highly complex, and cannot be used for fast applications due to their long computation time. As mentioned above, previous research in visibility computation has been devoted to open environments using Digital Elevation Model (DEM) models, representing raster data in 2.5D (Polyhedral model), which do not address, or suggest solutions for, densely built-up areas

---

For our case, the initialized population of viewpoints configuration is set randomly, and would probably be a poor solution due to its random nature, as can be estimated. The chromosome is a  $3 \times N$ -dimensional vector for  $N$  sensor's locations, i.e. viewpoints, where position and translation is a 3-dimensional  $(x,y,z)$  vector for each viewpoint location, as seen in Figure 14. The population is depicted in Figure 15.

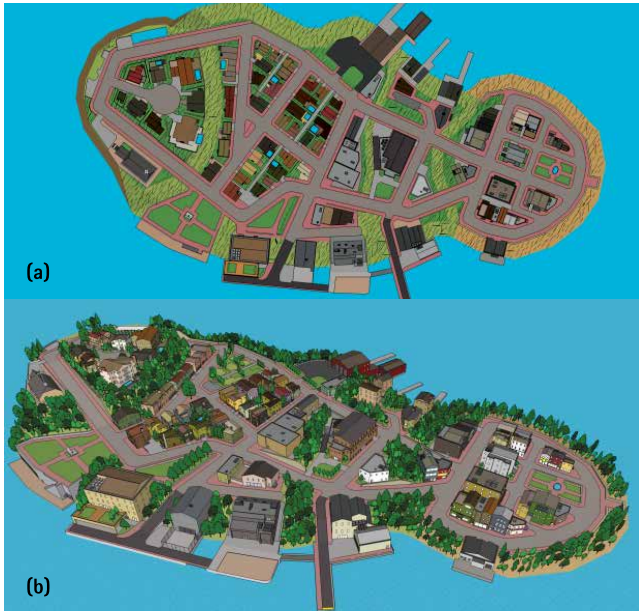


Figure 13: Fallville Island Sketchup Google Model Simulating Dense Urban Scene with Trees, [19]: (a) Topview; (b) Isometric view.



Figure 14: Bounded Area inside Bounding Box S marked in Black, inside Fallville Island Sketchup Google Model.



Figure 15: Bounded Polygons of Optimized Cover Viewpoints Using GA marked with Arrows.

**Evaluation:** The key factor of genetic algorithm relates to individual evaluation which is based on a score for each chromosome, known as Fitness function. This stage is the most time-consuming in our optimization, since we evaluate all individuals in each generation. It should be noticed that each chromosome score leads to 3D visible volume computation  $N$  times. As a tradeoff between the covered area and computational effort, we set  $N$  to eight. In the worst case, one generation evaluation demands visibility analysis for four thousand different viewpoints. In such a case, one can easily understand the major drawback of the GA method in relation to computational effort. Nevertheless, parallel computation has made a significant breakthrough over the last two decades; GA and other optimization methods based on independent evaluation of each chromosome can nearly be computed in linear time.

*Fitness Function* The fitness function evaluates each chromosome using optimization function, finding a global minimum value which allows us to compare chromosomes in relation to each other.

In our case, we evaluate each chromosome's quality using 3D visible volumes normalized to the bounding box  $S$  around a viewpoint:

$$f(i) = \frac{1}{S} \sum_{j=1}^N VV_S(x_j, y_j, z_j) \quad (4)$$

**Selection:** Once the population is sorted by fitness, chromosomes' population with greater values will have a better chance of being selected for the next reproduction stage. Over the last years, many selection operators have been proposed, such as the Stochastic Universal Sampling and Tournament Selection. We used the most common Tournament, where  $k$  individuals are chosen randomly, and the best performance from this group is selected. The selection operator is repeated until a sufficient number of parents are chosen to form a child generation.

**Reproduction:** In this stage, the parent individuals chosen in the previous step are combined to create the next generation. Many types of reproduction have been presented over the years, such as crossover, mutation and elitism.

Crossover takes parts from two parents and splices them to form two offspring, as seen in Figure 16(a). Mutation modifies the parameters of a randomly selected chromosome from within a single parent, as seen in Figure 16(b). Elitism takes the fittest parents from the previous generation and replicates them into the new generation. Finally, individuals not selected as parents are replaced with new, random offspring. Further analysis and operators can be found in [29][36]. The major steps of these operators can be seen in Figure 16.

## Simulations

In this section, we report on simulation runs with our 3D visible volumes analysis in urban scenes integrated with trees, using genetic algorithms. The genetic algorithms were tested on a 1.8GHz Intel Core CPU with Matlab. We used Fallville Island Sketchup Google Model [19] for simulating a dense urban scene with trees, as seen in Figure 17.

The stages of Crossover and Elitism operators are described as follows, with a probability of  $P_c=0.9$  (otherwise parents are copied without change):

1. Choose a random point on the two parents
2. Split parents at this crossover point
3. Create next generation chromosomes by exchanging tails

Where the Mutation operator modifies each gene independently with a probability of  $P_m=0.1$

In order to process the huge amount of data, we bounded a specific region which includes trees and buildings, as seen in Figure 18. We imported the chosen region to Matlab and modeled the objects by boxes, neglecting roofs' profiles. Time computation for one generation was one hour long on average. As we could expect, the evaluation stage took up 94% of the total simulation time. We set the bounding box S as [500 m\* 200 m\* 50 m]. Population initialization included 500 chromosomes, each of which is a 24-dimensional vector consisting of position and translation, where all of them were generated randomly.

Based on the Fitness function described previously and the different GA stages and 3D visible volumes analysis, the location of eight viewpoints for sensor placement was optimized. Viewpoints must be bounded in S and should not penetrate buildings and trees. Stop criteria was set to 50 generations and Fitness function gradient.

Optimal coverage of viewpoints and visible volumes during ten runnings'

---

For the first time we integrated trees as partially visible objects participating in a 3D visible volumes analytic analysis and conditions necessary for visibility with sensors' noises effects. As part of our research we tested several 3D models of 3D urban environments from the visibility viewpoint, choosing the best model from the computational effort and the analytic formulation aspects

---

simulations is seen in Figure 19, bounded in polygons marked with arrows. During these ten runnings simulations, we initialized the population randomly at different areas inside bounding box S.

These interesting results show that trees' effect inside a dense urban environment was minor, and trees around the buildings in open spaces set the viewpoint's location. As seen in Figure 19, polygon A and polygon B are both outside the areas blocked by buildings. But they are still located near trees, which affect the visible volumes, and we can predict that the same affect will occur in our real world. On the other hand, polygon C, which is closer to the area blocked by buildings, takes into account the trees in this region, but the major factor are still the buildings.

## Conclusions

In this paper, we presented an optimized solution for the problem of computing maximal coverage from a number of viewpoints, using a genetic algorithms method. In addition, we propose the conditions necessary for visibility based on sensors' model analysis, taking into account stochastic character. As far as we know, for the first time we integrated trees as partially visible objects participating in a 3D visible volumes analytic analysis and conditions necessary for visibility with sensors' noises effects. As part of our research we tested several 3D models of 3D urban environments from the visibility viewpoint, choosing the best

model from the computational effort and the analytic formulation aspects.

We tested our 3D visible volumes method on real a 3D model from an urban street in the city of Haifa, with time computation and visible volumes parameters.

In the second part of the paper, we introduced a genetic algorithm formulation to calculate an optimized solution for the visibility problem. We used several reproduction operators, which made our optimization robust. We tested our algorithm on the Fallville Island Sketchup Google Model combined with trees, and analyzed the viewpoint's polygons results, and also compared using versus not using the conditions necessary for visibility. Based on our results, an optimal trajectory can be planned by using an optimal visibility points as basic global search results, adding local permutations over it.

Our future work is related to validation between our simulated solution and projected volumes from sensors mounted in these viewpoints for optimal coverage.

## References

- [1] O. Gal and Y. Doytsher, "Sensors Placement in Urban Environments Using Genetic Algorithms," The Seventh International Conference on Advanced Geographic Information Systems, Applications, and Services, pp. 82-87, 2015.

- [2] N. Abu-Akel, "Automatic Building Extraction Using LiDAR Data," PhD Dissertation, Technion, Israel, 2010.
- [3] D. Cohen-Or, G. Fibich, D. Halperin and E. Zadicario, "Conservative Visibility and Strong Occlusion for Viewspace Partitioning of Densely Occluded Scenes," In EUROGRAPHICS'98.
- [4] D. Cohen-Or and A. Shaked, "Visibility and Dead- Zones in Digital Terrain Maps," Eurographics, vol. 14, no. 3, pp.171-180, 1995.
- [5] R. Cole and M. Sharir, "Visibility Problems for Polyhedral Terrain," Journal of Symbolic Computation, vol. 7, pp.11-30, 1989.
- [6] K. Chakrabarty, S. Iyengar, H. Qi and E. Cho, "Grid Coverage for Surveillance and Target Location in Distributed Sensor Networks," IEEE Trans. Comput, vol. 51, no. 12, 2002.
- [7] Y. Chrysanthou, "Shadow Computation for 3D Interactive and Animation," Ph.D. Dissertation, Department of Computer Science, College University of London, UK, 1996.
- [8] R. Church and C. ReVelle, "The Maximal Covering Location Problem," Papers of the Regional Science Association, vol. 32, pp.101-118, 1974.
- [9] T. Clouqueur, V. Phipatanasuphorn, P. Ramanathan and K.K. Saluja, "Sensor deployment strategy for target detection," In WSN, 2002.
- [10] T. Clouqueur, K.K. Saluja and P. Ramanathan, "Fault tolerance in collaborative sensor networks for target detection," IEEE Trans. Comput, vol. 53, no. 3, 2004.
- [11] L. De Florian and P. Magillo, "Visibility Algorithms on Triangulated Terrain Models," International Journal of Geographic Information Systems, vol. 8, no. 1, pp.13-41, 1994.
- [12] L. De Florian and P. Magillo, "Intervisibility on Terrains," In P.A. Longley, M.F. Goodchild, D.J. Maguire & D.W. Rhind (Eds.), Geographic Information Systems: Principles, Techniques, Management and Applications, pp. 543-556. John Wiley & Sons, 1999.
- [13] Y. Doytsher and B. Shmutter, "Digital Elevation Model of Dead Ground," Symposium on Mapping and Geographic Information Systems (ISPRS Commission IV), Athens, Georgia, USA, 1994.
- [14] G. Drettakis and E. Fiume, "A Fast Shadow Algorithm for Area Light Sources Using Backprojection," In Computer Graphics (Proceedings of SIGGRAPH '94), pp. 223-230, 1994.
- [15] M.F. Duarte and Y.H. Hu, "Vehicle classification in distributed sensor networks," Journal of Parallel and Distributed Computing, vol. 64, no. 7, 2004.
- [16] F. Durand, "3D Visibility: Analytical Study and Applications," PhD thesis, Universite Joseph Fourier, Grenoble, France, 1994.
- [17] A.E. Eiben and J.E. Smith, "Introduction to Evolutionary Computing Genetic Algorithms," Lecture Notes, 1999.
- [18] U.M. Erdem and S. Sclaroff, "Automated camera layout to satisfy task- specific and floor plan-specific coverage requirements," Computer Vision and Image Understanding, vol. 103, no. 3, pp. 156-169, 2006.
- [19] Fallvile, (2010) <http://sketchup.google.com/3dwarehouse/details?mid=2265cc05839f0e5925ddf6e8265c857c&prevstart=0>
- [20] D. Fisher-Gewirtzman, A. Shashkov and Y. Doytsher, "Voxel Based Volumetric Visibility Analysis of Urban Environments," Survey Review, DOI: 10.1179/1752270613Y.0000000059, 2013.
- [21] W.R. Franklin, "Siting Observers on Terrain," in D. Richardson and P. van Oosterom, eds, Advances in Spatial Data Handling: 10th International Symposium on Spatial Data Handling. Springer-Verlag, pp. 109-120, 2002.
- [22] W.R. Franklin and C. Ray, "Higher isn't Necessarily Better: Visibility Algorithms and Experiments," In T. C. Waugh & R. G. Healey (Eds.), Advances in GIS Research: Sixth International Symposium on Spatial Data Handling, pp. 751-770. Taylor & Francis, Edinburgh, 1994.
- [23] W.R. Franklin and C. Vogt, "Multiple Observer Siting on Terrain with Intervisibility or Loes Data," in XXth Congress, International Society for Photogrammetry and Remote Sensing. Istanbul, 2004.
- [24] H. Furuta, K. Maeda and E. Watanabe, "Application of Genetic Algorithm to Aesthetic Design of Bridge Structures," Computer-Aided Civil and Infrastructure Engineering, vol. 10, no. 6, pp.415-421, 1995.
- [25] O. Gal and Y. Doytsher, "Analyzing 3D Complex Urban Environments Using a Unified Visibility Algorithm," International Journal On Advances in Software, ISSN 1942-2628, vol. 5 no.3&4, pp:401-413, 2012.
- [26] O. Gal and Y. Doytsher, "Dynamic Objects Effect on Visibility Analysis in 3D Urban Environments," Lecture Notes in Computer Science (LNCS), vol. 7820, pp.147-163, DOI 10.1007/978-3-642-37087-8\_11, Springer, 2013.
- [27] O. Gal and Y. Doytsher, "Spatial Visibility Clustering Analysis In Urban Environments Based on Pedestrians' Mobility Datasets," The Sixth International Conference on Advanced Geographic Information

- Systems, Applications, and Services, pp. 38-44, 2014.
- [28] H. González-Bañós and J.C. Latombe, "A randomized art-gallery algorithm for sensor placement," in ACM Symposium on Computational Geometry, pp. 232-240, 2001.
- [29] D.E. Goldberg and J.H. Holland, "Genetic Algorithms and Machine Learning," Machine Learning, vol. 3, pp.95-99, 1998.
- [30] Holden (2013), <http://slog.thestranger.com/slog/archives/2013/04/21/after-the-boston-bombings-do-american-cities-need-more-surveillance-cameras>
- [31] J. Holland, "Adaptation in Natural and Artificial Systems," University of Michigan Press, 1975.
- [32] D. Li and Y.H. Hu, "Energy based collaborative source localization using acoustic micro-sensor array," EURO SIP J. Applied Signal Processing, vol. 4, 2003.
- [33] D. Maddalena and G. Snowdon, "Applications of Genetic Algorithms to Drug Design," In Expert Opinion on Therapeutic Patents, pp. 247-254, 1997.
- [34] M. Mäntylä M, "An Introduction to Solid Modeling," Computer Science Press Rockville, Maryland, 1988.
- [35] M. Marengoni, B.A. Draper, A. Hanson and R. Sitaraman, "A System to Place Observers on a Polyhedral Terrain in Polynomial Time," Image and Vision Computing, vol. 18, pp.773-780, 2000.
- [36] M. Mitchell, "An Introduction to Genetic Algorithms (Complex Adaptive Systems)," MIT Press, 1998.
- [37] B. Nadler, G. Fibich, S. Lev-Yehudi D. and Cohen-Or, "A Qualitative and Quantitative Visibility Analysis in Urban Scenes," Computers & Graphics, vol. 5, pp.655-666, 1999.
- [38] G. Nagy, "Terrain Visibility, Technical report," Computational Geometry Lab, ECSE Dept., Rensselaer Polytechnic Institute, 1994.
- [39] K.J. Obermeyer, "Path Planning for a UAV Performing Reconnaissance of Static Ground Targets in Terrain," in Proceedings of the AIAA Guidance, Navigation, and Control Conference, PP.1-11, 2009.
- [40] K. Omasa, F. Hosoi, T.M. Uenishi, Y. Shimizu and Y. Akiyama, "Three-Dimensional Modeling of an Urban Park and Trees by Combined Airborne and Portable On-Ground Scanning LIDAR Remote Sensing," Environ Model Assess vol. 13, pp.473-481, DOI 10.1007/s10666-007-9115-5, 2008.
- [41] H. Plantinga and R. Dyer, "Visibility, Occlusion, and Aspect Graph," The International Journal of Computer Vision, vol. 5, pp.137-160, 1990.
- [42] C. Ratti, "The Lineage of Line: Space Syntax Parameters from the Analysis of Urban DEMs," Environment and Planning B: Planning and Design, vol. 32, pp.547-566, 2005.
- [43] H. Samet, "Hierarchical Spatial Data Structures," Symposium on Large Spatial Databases (SSD), pp. 193-212, 1989.
- [44] G. Schaufler, J. Dorsey, X. Decoret and F.X. Sillion, "Conservative Volumetric Visibility with Occluder Fusion," In Computer Graphics, Proceedings of SIGGRAPH, pp. 229-238, 2000.
- [45] V. Shaferman and T. Shima, "Coevolution genetic algorithm for UAV distributed tracking in urban environments," in ASME Conference on Engineering Systems Design and Analysis, 2008.
- [46] A. Streilein, "Digitale Photogrammetrie und CAAD," Ph.D Thesis, Swiss Federal Institute of Technology (ETH) Zürich, Diss. ETH Nr. 12897, Published in Mitteilungen Nr. 68 of the Institute of Geodesy and Photogrammetry, 1999.
- [47] J. Stewart and S. Ghali, "Fast Computation of Shadow Boundaries Using Spatial Coherence and Backprojections," In Computer Graphics, Proceedings of SIGGRAPH, pp. 231-238, 1994.
- [48] S.J. Teller, "Computing the Antipenumbra of an Area Light Source," Computer Graphics, vol. 26, no.2, pp.139-148, 1992.
- [49] D. Tian and N.D. Georganas, "A coverage-preserved node scheduling scheme for large wireless sensor networks," In WSNA, 2002.
- [50] E.P.K. Tsang and J. Li, "Combining Ordinal Financial Predictions with Genetic Programming," In Proceedings of the Second International Conference on Intelligent Data Engineering and Automated Learning, pp. 532-537, 2000.
- [51] P. Varshney, "Distributed Detection and Data Fusion," Springer-Verlag, 1996.
- [52] J. Wang, G.J. Robinson and K. White, "A Fast Solution to Local Viewshed Computation Using Grid-based Digital Elevation Models," Photogrammetric Engineering & Remote Sensing, vol. 62, pp.1157-1164, 1996.
- [53] J. Wang, G.J. Robinson and K. White K, "Generating Viewsheds without Using Sightlines," Photogrammetric Engineering & Remote Sensing, vol. 66, pp. 87-90, 2000.

*The Paper prepared for presentation at the "2020 WORLD BANK CONFERENCE ON LAND AND POVERTY" The World Bank - Washington DC, March 16-20, 2020. ▽*

# Lessons learned from the modernization of the Greek cadastre – Principles and progress

The main objective of PDI is successful cadastral projects delivery. Toward this goal, PM Framework provides validated information which supports decision making by the HC top management and the Ministry. The benefits of endorsing the PM approaches on cadastral projects are close schedule monitoring and control, the improvement of QA/QC, proactive performance and risk management as well as effective stakeholder engagement



**Aristeia Ioannidi**  
Rural Et Surveying  
Engineer, Director of  
Projects Directorate  
HELLENIC CADASTRE,  
Greece



**Maria Fouskolagoudaki**  
Maria Fouskolagoudaki  
Rural Et Surveying  
Engineer, MBA, PMP  
HELLENIC CADASTRE  
Head of Design,  
Specification Et  
Procurement Division  
Projects Directorate,  
Greece

## Introduction

The development of the modern Greek cadaster has been a long standing objective for every Greek government since the early 19th century in order to replace the existing old-fashioned individual based system of deeds registration rather than parcel based system, administered by a nationwide network of independent or state owned Registration and Mortgage Offices, under the loose supervision of Ministry of Justice.

In 1995, a new law was enforced, describing the procedure for the cadaster creation, providing that the claimants will make statements of their properties, submitting the necessary documents. According to the provisions of the new law, Greece set up a program of systematically creating an integrated cadaster, assisted by geospatial infrastructure, combining the property rights with the parcel, launching pilot programs covering

several municipalities through out the country. This was so difficult a task because of the complicated property status in Greece and the large number of stakeholders involved (individuals, public property management agencies, forest agencies and numerous other beneficiaries). The program has evolved in four Stages. The 1st Stage included pilot projects (1995 – 1998), the 2nd Stage urban centers (2008), 3rd Stage suburban and rural areas (2011) and the 4th Stage included the remainder of Greece, covering mostly rural areas.

Since 2016, the Greek government decided to accelerate the completion of Greek cadaster, awarding 32 cadastral contracts, covering the remainder of the country (65% of total country area and 44% of total country rights).

Hellenic Cadaster has acquired a lot of experience and has learned from its successes and failures of the past 25 years. The completion of Greek cadaster is a huge endeavor aiming to create a modern cadaster, using state of the art technologies including an on line application for collecting and assessing statements, an application for uploading reports and deliverables, as well as electronic applications for the submission of statements.

Cadastral creation stages				
	1998	2008	2011	2016
Number of contracts	64	37	35	32
Area (km <sup>2</sup> )	8.302	3.573	34.245	85.573
Rights (m)	6,7	8,2	6,9	17,3
Budget (m €)	233 m €	203 m €	297 m €	310 m €

## Materials and methods

### Management tools development

- **PMIS (Projects Management Information System) :**

A tailor-made PMIS , web app, has been designed by HC personnel and the experts of WB for managing and reporting on cadastral projects and assisting project managers, the PMO and the top management of the HC.

**Functionalities of the PMIS:**

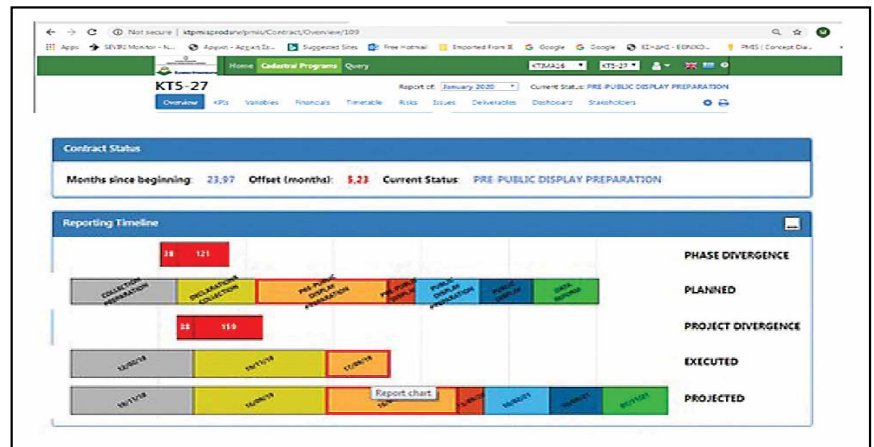
Contract information on cadastral projects, on line linkage to the central cadastral DB, on line data on the progress of statement collection/appeals submission, monitor the progress of the cadastral works (time, cost, scope) using several variables, deliverables QA/QC, monitor the progress of the cadastral contracts against the baseline using KPIs, risk management (assessment/monitor), issue monitoring, projects managers monthly reports on project, built-in queries to extract any data incorporated in the system.

- **The Projects Portfolio Development Initiative (PDI) of the Hellenic Cadaster Projects Directorate:**

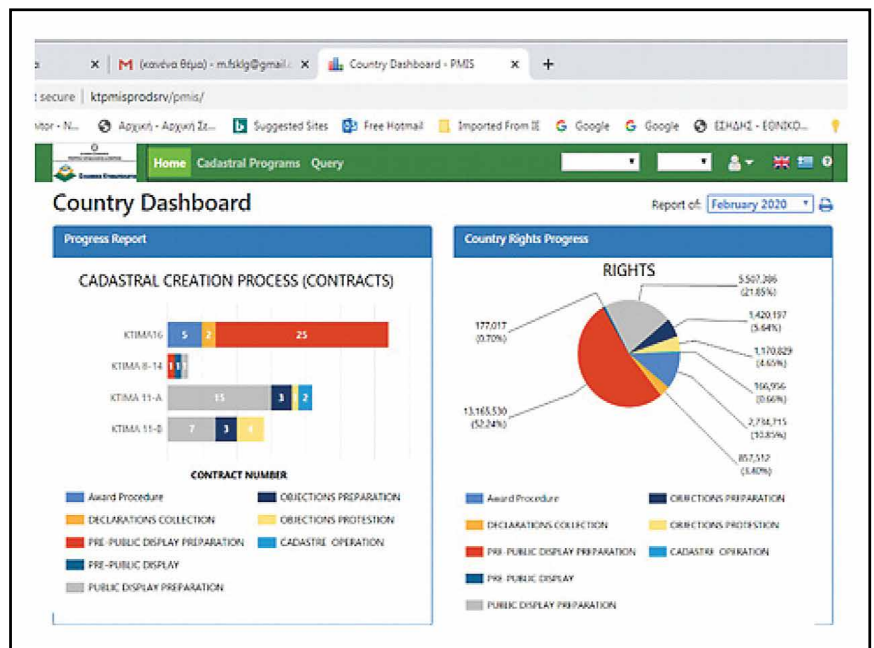
As the functional structure of HC was hindering the projects delivery, a PDI has been established in the Project Directorate, based on a tailored, flexible project management

framework incorporating international standardized project management

principles, processes, best practices and successful project delivery structures.



Project timeline



Country dashboard





## Conclusions

### Monitoring projects performance

The Projects Directorate has 65 cadastral projects in progress and soon 5 more contracts will be awarded, having 500 m € total budget. Given the complexity of the projects due to the large number of stakeholders involved in the cadastral projects and the constraints for the completion of the cadaster set by the government and EU for funding the projects, the close monitoring of the projects progress as well as the proactive approach to manage risks and resolve issues are very crucial.

### Decision making

The main objective of PDI is successful cadastral projects delivery. Toward

The benefits of endorsing the PM approaches on cadastral projects are close schedule monitoring and control, the improvement of QA/QC, proactive performance and risk management as well as effective stakeholder engagement

this goal, PM Framework provides validated information which supports decision making by the HC top management and the Ministry. Further analysis based on analytics and data processing is provided by the PMO to senior management.

The benefits of endorsing the PM approaches on cadastral projects are close schedule monitoring and control, the improvement of QA/QC, proactive

performance and risk management as well as effective stakeholder engagement.

### Things we can do better

Although a lot of progress has been made and the Ministry of the Environment has an overall picture for the performance and progress of the projects portfolio, there are still crucial issues and risks that need to be addressed like lack of sponsorship and skills gap. ▽

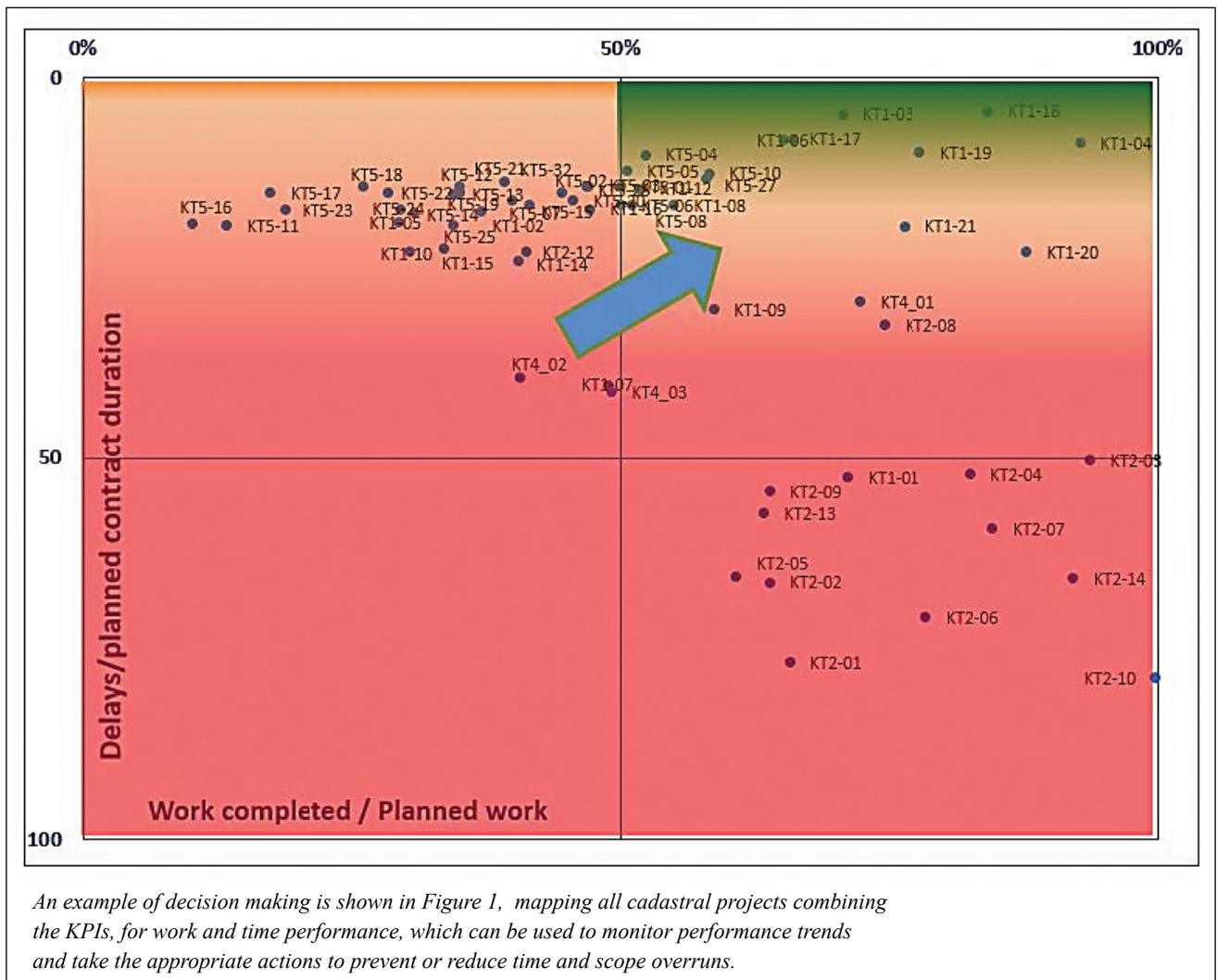


Figure 1 : Mapping of Cadastral Projects based on Time & Scope Performance

# What is readily available globally does not need to be regulated

Government of India has released the long awaited guidelines for acquiring and producing geospatial data and services including maps. We request our readers to share their views

## Preamble

Location information is an integral part of the modern digital ecosystem and critical for unlocking economic, social and environmental opportunities for sustainable growth and development of the country. It is critical to the success of modern industry offering location-based services such as e-Commerce, delivery and logistics and urban transport. It is also essential for more traditional sectors of the economy such as agriculture, construction and development and mines and minerals.

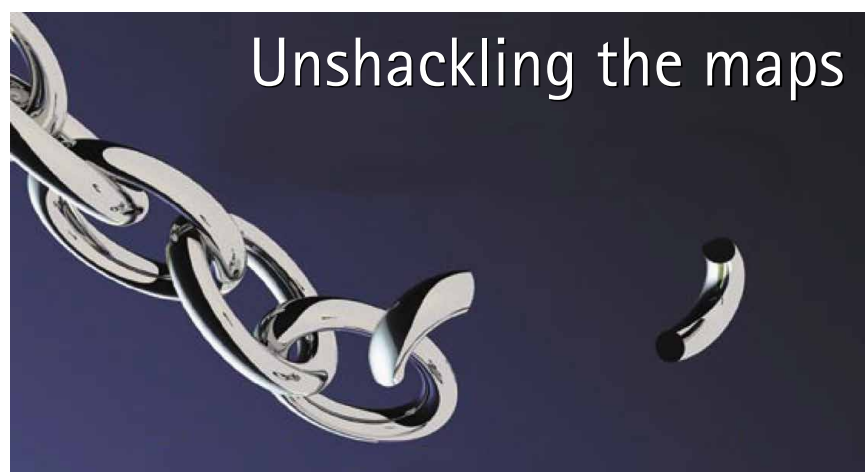
2. Geospatial data which includes location information are data about the natural or man-made, physical or imaginary features whether above the ground or below, boundaries, points of interest, natural phenomena, mobility data, weather patterns, statistical information, etc. There has been immense

progress over the years in technology for capture of geospatial data through ground-based survey techniques, photogrammetry using manned/ unmanned aerial vehicles, terrestrial vehicle mounted Mobile Mapping System, LIDAR, RADAR Interferometry, satellite-based remote sensing, mobile phone sensors and other techniques.

3. The Government of India acknowledges that the availability of comprehensive, highly accurate, granular and constantly updated representation of Geospatial Data will significantly benefit diverse sectors of the economy and will significantly boost innovation in the country and greatly enhance the preparedness of the country for emergency response.

## Atmanirbhar Bharat

4. The availability of data and modern mapping technologies to Indian companies is also crucial for achieving India's policy aim of Atmanirbhar Bharat and the vision for a five trillion-dollar economy. India presently relies heavily on foreign resources for mapping technologies and services. Liberalisation of the mapping industry and democratization of existing datasets will spur domestic innovation and enable Indian companies to compete in the global mapping ecosystem by leveraging modern geospatial technologies. Locally available and locally relevant Maps and Geospatial Data would also help in improved planning and management of



---

There shall be a negative list of sensitive attributes that would require regulation before anyone can acquire and/or use such attribute data. DST will notify this list on its website along with stipulated regulations after consultation with departments concerned

---

resources and better serve the specific needs of the Indian population.

5. Blue economy in India is another sunrise issue for development experts where Geospatial Data is expected to play a potentially important role. Fisheries, deep sea mining, and offshore oil and gas make up a large section of India's blue economy. The Sagarmala project, launched by the Government of India, is the strategic initiative for port-led development. India will soon launch an ambitious 'Deep Ocean Mission' that envisages exploration of minerals, energy and marine diversity of the underwater world, a vast part of which still remains unexplored.

Bathymetric Geospatial Data would be crucial for attainment of a flourishing and vibrant blue economy for the country and would require active participation of private sector in acquisition and their use apart from traditional agencies like Navy, etc.

6. With the advent of publicly available geospatial services, a lot of Geospatial Data that used to be in restricted zone are freely and commonly available now and some of the policies/guidelines that used to regulate such information have been rendered obsolete and redundant. What is readily available globally does not need to be regulated.

### Definitions:

7. (a) Positional data: Latitude, longitude and elevation/depth of a point or its x, y & z co-ordinates in the territory of the Republic of India.

(b) Attribute data: Any data that when associated with Positional Data gives any additional meaning to it.

(c) Geospatial Data: Positional data with or without attribute data tagged, whether in the form of images, videos, vector, voxel and/or raster datasets or any other type of geospatial dataset in digitized or non-digitized form or web-services.

(d) Map: Symbolic representation of real-world objects, regions or themes on a given scale which was generally published in paper form but now also available as web-map-service.

(e) Geospatial Technology: Any technology including but not limited to Aerial / UAV Photogrammetry, Aerial / UAV LIDAR, drones, Radar Interferometry, street view or by other means of ground survey, satellite-based remote sensing techniques, AI, underwater mapping, and others.

(f) Indian Entity: Any Indian citizen,

Government entities, Societies registered under applicable statutes, statutory bodies, Autonomous Institutions of the Government, or any Indian company or Indian LLP owned by resident Indian citizens or any Indian company or Indian LLP controlled by resident Indian citizens (as defined in the Explanation to Rule 23 of the Foreign Exchange Management (Non-Debt Instrument) Rules, 2019).

### Liberalisation of acquisition and production of geospatial data and geospatial data services including maps:

8. Accordingly, the following guidelines on acquiring and producing geospatial data and geospatial data services are issued in supersession of anything to the contrary on the subject issued from time to time by Department of Science and Technology (DST), Ministry of Defense (MoD) and/or any other Department of Government of India vide their various official memoranda and guidelines. The Guidelines issued by DST on Geospatial Data and Maps would be the single point reference on the subject.

- i. These guidelines will be applicable to Geospatial Data, Maps, products, solutions and services offered by government agencies, autonomous bodies, academic and research institutions, private organizations, Non- Governmental Organizations and individuals.

---

Indian Entities, whether in Government or outside, will be free to acquire, collect, generate, prepare, disseminate, store, share, publish, distribute, update, digitize and/or create Geospatial Data, including Maps, of any spatial accuracy within the territory of India including underwater within its territorial waters by using any Geospatial Technology, subject to regulations on attributes in the negative lists

---

---

Digital Maps/Geospatial Data of spatial accuracy/value up to the threshold value can be uploaded to the cloud but those with accuracy finer than the threshold value shall only be stored and processed on a domestic cloud or on servers physically located within territory of India

---

- ii. (1) Save as specifically provided for under these guidelines, there shall be no requirement for prior approval, security clearance, license or any other restrictions on the collection, generation, preparation, dissemination, storage, publication, updating and/or digitization of Geospatial Data and Maps within the territory of India. Individuals, companies, organizations, and Government agencies, shall be free to process the acquired Geospatial Data, build applications and develop solutions in relation to such data and use such data products, applications, solutions, etc. by way of selling, distributing, sharing, swapping, disseminating, publishing, deprecating and destructing. Self-certification will be used to convey adherence to these guidelines.  
(2) Nothing contained in these guidelines shall confer on any individual or an entity a right to physical access including through aerial/territorial water route to any establishment, installation or premises to which access is restricted by the Ministry/ Department concerned as the owner of such premises.
- iii. (a) There shall be a negative list of sensitive attributes that would require regulation before anyone can acquire and/or use such attribute data. DST will notify this list on its website along with stipulated regulations after consultation with departments concerned.  
(b) The negative lists mentioned above will be specific to very sensitive attributes and care

would be taken so as to minimize restrictions in order to boost the Ease of Doing Business. The list may be regularly updated as required.  
(c) DST will constitute a Geospatial Data Promotion and Development Committee with representations from relevant departments that would decide any issue arising out of finalization of negative attributes lists and the regulations proposed on those attributes. The Committee's mandate will include promotion of activities related to collection, generation, preparation, dissemination, storage, publication, updating and/or digitization of Geospatial Data.

**Explanation:**

- (1) There will not be any negative list of prohibited areas.
- (2) The negative list of attributes will include attributes that shall not be marked on any Map i.e. no person or legal entity shall identify or associate any location on a Map with a prohibited attribute.
- iv. (a) For the purposes of these guidelines, the threshold value for:
  - 1. On-site spatial accuracy shall be one meter for horizontal or Planimetry and three meters for vertical or Elevation. Gravity anomaly shall be 1 milli-gal.
  - 2. Vertical accuracy of Bathymetric data in Territorial Waters shall be 10 meters for up to 500 meters from the shore-line and 100 meters beyond that.
- (b) For the attributes in the negative list, different threshold values as well as regulations as warranted can be laid

- down. The thresholds shall be regularly reviewed and amended as necessary by DST.
- v. Indian Entities, whether in Government or outside, will be free to acquire, collect, generate, prepare, disseminate, store, share, publish, distribute, update, digitize and/or create Geospatial Data, including Maps, of any spatial accuracy within the territory of India including underwater within its territorial waters by using any Geospatial Technology, subject to regulations on attributes in the negative lists.
- vi. (a) Ground truthing/verification, access to Indian ground stations and augmentation services for real time positioning (Continuously Operating Reference Stations (CORS), etc.) and their data shall be made available without any restrictions and with the ease of access to Indian Entities only.  
(b) Terrestrial Mobile Mapping survey, Street View survey and surveying in Indian territorial waters

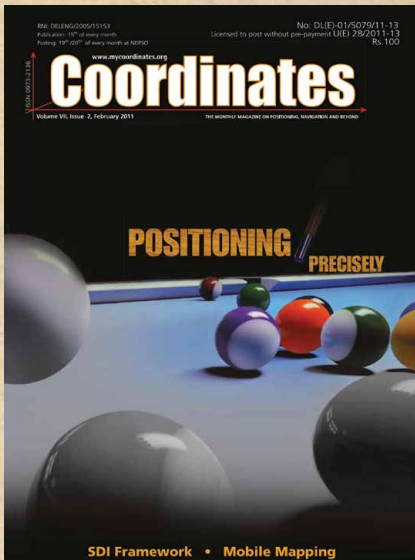
---

Save as specifically provided for under these guidelines, there shall be no requirement for prior approval, security clearance, license or any other restrictions on the collection, generation, preparation, dissemination, storage, publication, updating and/or digitization of Geospatial Data and Maps within the territory of India

---



# In Coordinates



mycoordinates.org/vol-7-issue-2-February-2011

10 years before...

## Continuous high precision navigation

**Yong li**

School of Surveying and Spatial Information Systems, University of New South Wales, Sydney, Australia

**Augustine Tsai**

Institute for Information Industry, Taipei, Taiwan

**Peter Mumford**

School of Surveying and Spatial Information Systems, University of New South Wales, Sydney, Australia

**Wei-sen Lin**

Institute for Information Industry, Taipei, Taiwan  
I-chou Hong, Institute for Information Industry, Taipei, Taiwan

An inexpensive integrated positioning device has been built for the I3 mobile mapping system. Tests conducted in both Sydney and Taipei demonstrate that the integration of RTK-GPS and MEMS inertial sensors can provide continuous position data in difficult environments with sufficient accuracy. Further tests will compare the NavExplorer solution with a solution of a higher accuracy.

## Seamless WLAN/GPS hybrid localization

**Young Jun Lee, Hee Sung Kim and Hyung Keun Lee**

School of Electronics, Telecomm. & Computer Eng., Korea Aerospace University, South Korea

To design a seamless and accurate localization method applicable to indoor/outdoor transit area of buildings, it is necessary to investigate measurement. By measurement collection and analysis, it was found that high-sensitivity GPS receivers provide sufficient number of measurements but with considerable multipath errors. It was also found that sufficient number of WLAN signals can be obtained nearby buildings but should be treated by considering NLOS errors.

## Real time precise-point-positioning

**María D, Láinez Samper**

R&D&I responsible in the GNSS Business Unit, GMV, Spain

**Miguel M Romay Merino**

GNSS Business Unit Director, GMV, Spain

**Álvaro Mozo García**

GNSS Algorithms and Products Division Head, GMV, Spain

**Ricardo Píriz Nuñez**

GNSS Product Manager, GMV, Spain

**Tsering Tashi**

System Engineer, ISRO Satellite Centre, India

GMV has developed magicPPP, an infrastructure ready to be used as COTS to be installed in any region of the world, which provides about the same accuracy as current RTK systems, both for static and dynamic users, requiring significantly less number of stations, reducing consequently the deployment and maintenance costs magicPPP works with a regional network of stations, and is highly flexible for selecting the location of the stations facilitating the possibility of doing precise positioning in remote areas.

Regional navigation constellations can be used for some PPP purposes, such as scientific applications, demanding high precision but in which the convergence time is not the most stringent requirement.

## NASA advancing GNSS capabilities

NASA is developing capabilities that will allow missions at high altitudes to take advantage of signals from Global Navigation Satellite System (GNSS) constellations — like GPS commonly used in the U.S. These signals — used on Earth for navigation and critical timing applications — could provide NASA’s Artemis missions to the Moon with reliable timing and navigation data. NASA’s Space Communications and Navigation (SCaN) program is developing the technologies that will support this goal.

Interoperability of the GNSS constellations will be key to realizing this ambition. There are six GNSS constellations that provide Position, Navigation, and Timing (PNT) services, each hailing from different countries worldwide. Four constellations, those operated by the U.S., the European Union, Russia, and China, provide global coverage. The other two, operated by India and Japan, provide regional coverage.

Using multiple constellations at once offers more signal availability, which can mean improved accuracy in navigation and timing for satellites. This could be especially helpful for spacecraft at higher altitudes where GNSS signals are less plentiful overall.

However, each constellation has unique designs. This poses a challenge to engineers hoping to develop multi-GNSS systems that take advantage of multiple constellations.

### Bobcat-1

SCaN is supporting a number of flight experiments that will help develop multi-GNSS capabilities for spacecraft. Bobcat-1, developed by NASA’s Glenn

Research Center in Cleveland and Ohio University, is one such example.

Bobcat-1 was selected by the CubeSat Launch Initiative in 2018 to study GNSS signals from 250 miles overhead. The small satellite launched to the International Space Station aboard a Northrop Grumman Cygnus spacecraft on Oct. 2, 2020.

On Nov. 5, the space station released the CubeSat to begin its mission. The spacecraft will orbit for about nine months, measuring signals from different GNSS constellations. Engineers will use these measurements to better understand GNSS performance, specifically focusing on timekeeping variations between the constellations.

### The SCaN Testbed

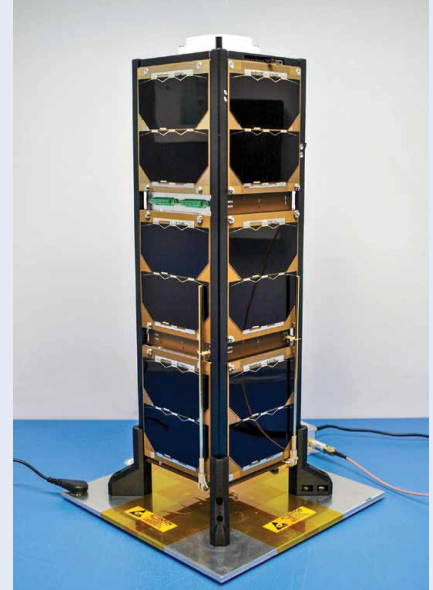
Bobcat-1 builds on the legacy of the SCaN Testbed, which demonstrated multi-GNSS capabilities on the space station from 2012 to 2019. The GPS and Galileo Receiver for the International Space Station (GARISS) — an instrument developed in collaboration between NASA and ESA (European Space Agency) — received signals from both GPS and Galileo, the GNSS constellation operated by the European Union.

The SCaN TestBed also laid the foundation for the Lunar GNSS Receiver Experiment (LuGRE), a Commercial Lunar Payload Services payload being developed in partnership with the Italian Space Agency. The payload will receive signals from both GPS and Galileo and is expected to obtain the first-ever GNSS fix on the lunar surface.

### GNSS PNT policy and advocacy

While NASA engineers develop the technologies necessary for multi-GNSS

Navigation Office. The four newly-released technical standards are for fields of the data format, map application, ground-based augmentation system and atomic clock of the BDS. These new technical standards have been released by the Standardization Administration.



Bobcat-1 with its deployable antenna stowed. Bobcat-1 will experiment with the GNSS inter-constellation time offset from low-Earth orbit. GNSS time-offset estimations are critical for users with a limited visibility of GNSS satellites, such as users at high altitudes. **Credits: NASA**

navigation at ever-higher altitudes, the SCaN team works with stakeholders in the U.S. government and internationally to advance GNSS interoperability in the policy sphere. They consult on the United Nations International Committee on GNSS, helping develop additional capabilities in the Space Service Volume and beyond.

NASA recently worked to publish GPS antenna patterns from GPS satellites that launched between 1997 and 2000, collaborating with the U.S. Space Force, the U.S. Coast Guard, and Lockheed Martin, who built the satellites. The PNT team is also working to facilitate publication of antenna patterns for more recent GPS satellites. With this data, mission planners can better assess the performance of GNSS in high-Earth orbit and lunar space. This forthrightness also encourages other GNSS providers to be similarly transparent. *By Danny Baird, NASA*. 

## China releases 4 new BDS technical standards

China has newly released four national technical standards for the BeiDou Navigation Satellite System (BDS), according to the China Satellite

China officially commissioned BDS on July 31, 2020, opening the new BDS-3 system to global users.

Along with positioning, navigation and timing services, the BDS-3 system can provide a variety of value-added

services like global search and rescue assistance, short message communication, ground-based and satellite-based augmentation, as well as precise point positioning. [www.xinhuanet.com](http://www.xinhuanet.com)

---

## Galileo Open Service Navigation Message Authentication

Galileo has started testing Open Service Navigation Message Authentication (OSNMA) in the signal-in-space, allowing the first-ever OSNMA-protected position fix to be successfully computed. Testing will continue over the next months, ahead of a so-called “public observation” phase. This is the first-ever transmission of authentication features in open GNSS signals of a global navigation system.

The Galileo OSNMA is an authentication mechanism that allows GNSS receivers to verify the authenticity of GNSS information, making sure that the data they receive are indeed from Galileo and have not been modified in any way. On November 18th 2020, 15:28 UTC, Galileo satellites started the transmission of authentication data for testing purposes. As part of the tests, OSNMA receivers successfully calculated a message-authenticated position for the first time.

### Testing Activities

OSNMA test signals are being broadcast by the Galileo constellation using the spare bits from the current navigation message, therefore not impacting the legacy OS receivers implementing the current OS Signal-In-Space Interface Control Document (OS SIS ICD). The first tests used eight Galileo satellites for around two hours on November 18th.

### Next steps

Upon successful completion of the internal testing phase, a public observation phase will begin, in which the OSNMA signal will be publicly accessible. In preparation of this phase, the OSNMA SIS ICD, receiver implementation guidelines, and the necessary cryptographic materials will be published. This will allow

receiver manufacturers and application developers to test and prepare their products. <https://ec.europa.eu>

---

## Establishing the framework for developing the Galileo PRS military user segment

A crucial and decisive step towards the development of the Galileo Public Regulated Service (PRS) military User Segment has been taken recently with the kick off meeting of the GEODE (Galileo for EU Defence) project.

This project managed under the aegis of the Belgian, French, German, Italian and Spanish Ministries of Defence is one of the most ambitious Defence cooperation projects launched under the umbrella of the European Defence Industrial Development Programme (EDIDP) of the European Commission. GEODE is also the biggest Galileo application development project ever launched. Sponsored by Belgium, Germany, Italy, France and Spain which contributions should exceed 82.7 million Euros, it is supported by the EU with a grant of about 44 million Euros.

GEODE is establishing the framework for developing the Galileo PRS user segment for Defence applications. The setting up of this framework starts already with the involvement of 30 companies and organisations from 14 EU Member States: Belgium, Czech Republic, Estonia, Finland, France, Germany, Greece, Italy, the Netherlands, Poland, Portugal, Spain, Sweden and Romania.

National Defence organisations have thoroughly elaborated in close cooperation with Industry the complete roadmap for the Galileo PRS military user segment development. Starting from a significant specification and standardisation phase, GEODE will prototype, test and qualify 7 PRS Security Modules developed from various technologies, 9 PRS receivers (including 2 server-based variants), 4 GPS/Galileo PRS compatible anti-jamming Controlled Radiation Pattern Antennas. In addition, a common and standardized test environment will be developed as well as a

PRS infrastructure to ensure the availability of the security assets for operational testing. To complete this picture, military operational field testing will be organised on military platforms (naval, land and Drones) and timing and synchronisation system in (at least) Belgium, Czech Republic, France, Germany, Greece and Romania. A PRS solution for spacecraft will also be designed and prototyped.

Beyond paving the way for the equipment of EU Member States Defence forces with Galileo PRS, this military user segment developed, tested and certified in the frame of GEODE aims to be available for export towards third countries (which have the necessary PRS security agreements with the EU).

The GEODE project will be completed in 2026. [www.fdc.fr](http://www.fdc.fr)

---

## Next-gen European navigation overlay service

The European GNSS Agency, GSA, has awarded a €100 million (\$121 million) contract to Eutelsat Communications to develop and operate the agency’s next-generation EGNOS satellite navigation overlay service.

The European Geostationary Navigation Overlay Service (EGNOS) is used to improve the performance and accuracy of U.S. GPS signals. These signals can then be utilized for safety critical applications for aviation, maritime and land-based customers like railway and road management agencies.

With the Feb. 9 contract signing, the GSA has entrusted Paris-based Eutelsat with the development and operation of the agency’s next-generation EGNOS GEO-4 service. Also referred to as EGNOS Version 3, the new service will make several improvements on its predecessor including integrating signals from Galileo, Europe’s own navigation system. GEO-4 payload is the second EGNOS payload to be hosted aboard a Eutelsat satellite. The first, GEO-3, was launched aboard Eutelsat 5 West B in October 2019. [www.eutelsat.com](http://www.eutelsat.com)

## EU court suspends Galileo signing with Thales and Airbus

The European Court of Justice in Luxembourg suspended the signing of the €1.47 billion Galileo contracts with Thales Alenia Space and Airbus Defence and Space, Space Intel Report found out.

The scheduled signing for a dozen of second-generation Galileo satellites “has been suspended by order of the European Court of Justice (ECJ) following a protest filed by OHB SE, which was the losing bidder,” Space Intel Report’s Peter de Selding wrote.

The European Commission had awarded contracts for 12 new Galileo satellites (six each) for a total of €1.47 billion to Thales Alenia Space in Italy and Airbus Defence & Space in Germany in January. OHB, the manufacturer of the first Galileo generation of more than two dozen satellites, lost the bid for the next generation. <https://spacewatch.global>

## Passenger buses in Turkmenistan with GPS/GLONASS system

President of Turkmenistan Gurbanguly Berdimuhamedov held a digital video

In order to increase passenger traffic and improve the quality of services, the President of Turkmenistan has instructed transport department to purchase medium and small buses installed with cashless payment systems and GPS/GLONASS system, just like in passenger taxis and trucks, to widely introduce internet services and the sale of travel cards.

In order to provide high-quality services to passengers of city and suburban buses, President Gurbanguly Berdimuhamedov demanded to ensure timely commissioning of modern bus stations that are under construction in Balkan, Dashoguz, Lebap and Mary velayats. <https://business.com.tm/post/6643/turkmenistan-intends-to-purchase-passenger-buses-with-gpsglonass-system>

## Global Mapper v22.1

Blue Marble Geographics has released version 22.1 of Global Mapper. The version 22.1 release includes several enhancements to the software’s 3D Viewer including, a new ‘Save 3D Views’ function and 3D View navigation tools to target the camera on specific features and lock the pivot axis around a feature of interest. The data graphing and charting feature has been updated with support for creating graphs from multiple layers, and several new spatial operations functions have been added, including ‘Union’ and ‘Difference. [bluemarblegeo.com](http://bluemarblegeo.com)

## OS Maps launches in Australia

Ordnance Survey, UK has launched its walking and cycling app, OS Maps, in Australia. It is the first nation outside Britain to have access to OS Maps. The new app’s accurate mapping and routes will help people to explore more and create their own adventures on and off the beaten track. <https://osmaps.com>

## ISRO and MapmyIndia to build alternative to Google Maps

Indian Space Research Organisation (ISRO) and MapmyIndia has joined hands to come up with an indigenous alternative to Google Maps.

Rohan Verma, CEO of MapmyIndia said its user maps, apps and services would “integrate with ISRO’s huge catalogue of satellite imagery, and earth observation data, and would be a much better”. He took to LinkedIn to announce the venture saying, “MapmyIndia, being a responsible, local Indian company, ensures that its maps reflect the true sovereignty of the country, depicting India’s borders as per the government of India, and hosts its maps in India.” <https://indianexpress.com>

## Bluesky 3D building models drive efficiency

Water sector solution provider MWH Treatment is using the latest 3D computer modelling technology

to improve the delivery of major construction projects across the UK. Created by aerial mapping company Bluesky International, models are used throughout the lifecycle of projects; from the production of animations at the concept stage right through to Virtual Reality (VR) simulations for health and safety training. The 3D models are helping MWH Treatment drive efficiency and collaboration and have already been used on a number of developments including the Winchburgh upgrade works for Scottish Water and Thames Gateway Desal upgrade for Thames Water. [bluesky-world.com](http://bluesky-world.com)

## EU-China collaboration for international marine data sharing

EU-China collaborations on marine data and knowledge sharing took a new step forward with the signing of a Memorandum of Understanding (MoU) between the European Marine Observation and Data Network (EMODnet) and the National Marine Data and Information Service (NMDIS) of China.

The agreement consolidates the operational, technical and scientific collaboration which is already well underway, by providing a clear framework to advance the joint efforts through the EMOD-PACE and CEMDNET projects on three specific areas of collaboration: (i) the sharing of available in-situ, earth observation and modelled marine data, (ii) the exchange of knowledge and best practices related to marine data and information product R&D and associated technology, and (iii) the development and implementation of common work plans between NMDIS and EMODnet in relation to ocean reanalysis, seabed habitat mapping, ecological vulnerability and coastal zone adaptation.

This MoU outlines the initial areas and activities envisaged to be taken forward as part of the cooperation partnership, while this list can be updated over time with mutual agreement. It is intended to further stimulate the development of collective approaches and practices to address mutual

and global challenges and concerns in relation to international ocean governance and ocean marine data. <https://emodnet.eu>

### Geollect win UKHO innovation award

Geollect has won the UK Hydrographic Office's prestigious ADMIRALTY Marine Innovation Programme challenge.

UKHO is looking at ways their data can enhance marine insurance products and reduce maritime risk. The award is recognition of the potential of Geollect products to unlock and visualise their extensive library.

The data provided by UKHO will massively enrich the solutions in the marine insurance sector. Products like electronic charts, bathymetry, CATZOC, wreck locations, offshore infrastructure and conservation areas will all help provide context for vessel behaviour. [www.geollect.com](http://www.geollect.com)

### Ghana launches National Map of Forests and Land Use

The Forestry Commission of Ghana (FCG) has launched the National Map of Forests and Land Use. Marking a significant milestone in Ghana's commitment to build world-class earth observation expertise and the culmination of a three-year project, the development has been supported by Forests 2020, which is managed by Ecometrica, the downstream space information company, and supported by the UK Space Agency's International Partnership Programme.

The launch of the map is the latest in a series of initiatives to enhance sustainability across Ghana's key agricultural commodities, such as cocoa, and aims to end deforestation, while promoting forest restoration and protection throughout supply chains. It will be formally adopted as a national product for the use of climate reporting and zero deforestation supply chains in both the forest sector and for commodity exports. <https://ghana-national-landuse.knust.ourecosystem.com> . 

### Technology demonstrator microsatellite for Norway

The Norwegian Space Agency (NOSA) has awarded Space Flight Laboratory (SFL) of Canada a contract to develop the NorSat Technology Demonstrator (TD) microsatellite. With a primary mission of testing out new technologies in space, NorSat-TD will validate payloads and concepts from Norway, the Netherlands, France and Italy.

SFL, which developed the operational NorSat-1 and -2 microsatellites launched in 2017, as well as NorSat-3 expected to launch in Q2 2021, has been contracted to design and build the NorSat-TD spacecraft and perform integration and testing of all systems and payloads. NorSat-TD has completed its final design review and been slated for launch in 2022. [www.utias-sfl.net](http://www.utias-sfl.net)

### Color image from NEMO-HD microsatellite

Space-SI, the Slovenian Centre of Excellence for Space Sciences and Technologies, released the first multispectral image captured by its NEMO-HD Earth observation microsatellite just 16 days after launch. Built by Space Flight Laboratory (SFL) in collaboration with SPACE-SI, NEMO-HD is Slovenia's first microsatellite carrying a multispectral high-definition Earth observation instrument.

The Slovenia satellite was built on SFL's NAUTILUS microsatellite bus, which is an augmentation of SFL's NEMO bus that has been used for numerous successful microspace missions. With a mass of only 65 kg and dimensions of 60x60x30 centimeters, NEMO-HD captures multispectral (RGB/NIR) images that can be sharpened by a panchromatic channel to 2.8-meter resolution.

The satellite also collects high-definition video at 25 frames per second. The main instrument can be operated in real-time imaging mode, allowing an operator at mission control on the ground to view the utias feed as it is captured. [www.utias-sfl.net](http://www.utias-sfl.net)

### RAAMS bathymetric Lidar technology

Fugro has won a contract to capture bathymetric lidar of Northern Ireland's coastline as part of a project from the Department of Agriculture, Environment and Rural Affairs (DAERA) to create a detailed 3D elevation model of the coast.

The nearshore survey will acquire satellite-derived bathymetry (SDB) data and, for the first time in the UK, Rapid Airborne Multibeam Mapping System (RAMMS) shall be used to collect lidar bathymetry data.

Coastal flooding is a global concern due to rising sea levels and an increase in extreme storm events. To identify areas most at risk of coastal erosion and marine flooding, and those that may be under future threat, DAERA has commissioned a baseline study of Northern Ireland's 763 km of coastline. The resulting 3D model will help to inform policy makers, coastal managers, terrestrial planners, marine planners and other interested stakeholders. [www.fugro.com](http://www.fugro.com)

### Vegetation risk analysis of entire U.S. electric transmission grid

For the first time in history, vegetation encroachment risk to the entire publicly available U.S. transmission grid has been analyzed from space by the Berlin-based start-up LiveEO. In total, over 15,000 public satellite images were used to evaluate risk to 574,000 miles of electricity lines.

The analysis covers the detection of vegetation along the transmission grid, as well as the identification of grid segments that are exposed at dangerously close distances. These are some of the biggest challenges and operational cost factors for utility companies in maintaining their assets. Proven by studies vegetation is one of the main challenges for utilities globally, causing up to 56% of externally triggered power interruptions.

Besides the sole detection of vegetation distance from transmission grids, LiveEO is experienced in highly

accurate and efficient investigations of vegetation height, condition, and species determination to improve cycle trimming activities and dangerous tree removal while reducing vegetation management costs on transmission and distribution levels. [www.live-eo.com](http://www.live-eo.com)

---

### SatSure – Bellatrix to establish a high-resolution satellite constellation

On February 3rd, 2021, SatSure has signed a MoU with Bellatrix Aerospace to help place its payloads in the Low Earth Orbit (LEO). The satellites will host a novel on-board processor for in-orbit high-resolution data processing using SatSure's proprietary Deep Learning algorithms and ultra low-bandwidth data transmission on a microsatellite platform comprising of Bellatrix Aerospace's unique hybrid propulsion systems. The missions will be supported by Bellatrix Aerospace's agile satellite platform currently under development and powered by its unique hybrid propulsion technology.

SatSure, founded in 2016 with core business in enterprise AI-based software products and platforms, has seen a surge in demand post-COVID-19 for data insights and solutions based on high-resolution satellite imagery.

Bellatrix Aerospace is an IP driven company founded in 2015 and working on advanced spacecraft propulsion systems. [satsure.co](http://satsure.co)

---

### Agriculture-focused satellite constellation to be launched

EOS Data Analytics, announced plans to launch seven optical EOS SAT satellites into an LEO (Low Earth orbit) by the year 2024. By launching its own satellite imaging constellation, the company aims to establish a full satellite data production vertical – from direct imagery collection to processing, analysis, and delivery.

One of the key objectives of the new satellite constellation will be monitoring of farmlands, making this project the first of its kind oriented towards agriculture. 

---

### Hiber successfully launches second generation satellite

Hiber, the European satellite IoT company, recently launched Hiber Four satellite in space, via SpaceX's first rideshare mission of 2021 - Transporter-1. It is a second generation satellite developed and assembled by Hiber's engineers in its Amsterdam office. Hiber Four, and its sister satellite Hiber Three (launching in March), are half the volume (3U) of the previous generation, which reduces the mass and decreases the launch costs by up to 50%. The newest generation of satellites also have an on-board propulsion system allowing ground engineers to adjust the satellite's orbit. This ensures that Hiber Four, and its future descendants, avoid collisions and, importantly, de-orbit themselves at the end-of-life, making Hiber one of the most responsible CubeSat constellation operators in the world. [www.hiber.global](http://www.hiber.global)

---

### Energy optimization software package for robot fleets

WiBotic has launched Commander, a robot fleet energy management software package specifically designed for customers operating large robot fleets. It is an easy-to-use, intuitive platform used to visualize, configure, and optimize the delivery of energy throughout a fleet of robots, drones or any battery-powered device using WiBotic charging systems. It is also a robust API, giving operators the opportunity to fully control the charging function as a part of each robot's daily workflow.

Commander provides a bird's eye view of the fleet's charging infrastructure, including a visual display of charger availability and status, and historical information on which chargers are being utilized more than others. [www.wibotic.com](http://www.wibotic.com)

---

### AI technology to create bathymetry product

TCarta Marine has introduced a Global Satellite Derived Bathymetry (G-SDB)

product line developed with a new seafloor depth measurement technique that leverages Machine Learning and NASA ICESat-2 laser data. The first G-SDB offering covers the entire Red Sea – available now – with additional data sets rolled out through the end of this year.

G-SDB data sets contain bathymetric measurements to depths of more than 30 meters, depending on water clarity, at 10-meter resolution. The depth values for every 10m pixel are the combined result of numerous measurements, resulting in accuracy within 10% of depth or less, and providing a seamless water bottom surface map. G-SDB will be available globally for all oceans and seas, as well as large freshwater lakes where water conditions permit. [www.tcarta.com](http://www.tcarta.com)

---

### Honeywell and Idemia announce strategic alliance

Honeywell and IDEMIA have announced a strategic alliance to create and cultivate an intelligent building ecosystem that provides a more seamless and enhanced experience for operators and occupants alike. The alliance will integrate Honeywell's security and building management systems with IDEMIA's biometric-based access control systems to create frictionless, safer and more efficient buildings.

The Honeywell and IDEMIA alliance is intended to design solutions that will allow occupants to easily and securely have contactless engagement with a building – from vehicle recognition at the car park and automatic elevator calls to biometric-based access and personalized conference room settings. With a focus on security and data privacy, these next-generation solutions will provide occupants with a safer, more efficient and more enjoyable experience that will help building owners attract tenants. [www.honeywell.com](http://www.honeywell.com)

---

### Combined navigation and digital tracking tool

UK-based navigation services provider Novaco has developed a new all-

in-one navigation data and tracking product for commercial and leisure vessels. It delivers and integrates secure navigation data to the bridge, while also providing real-time tracking and vessel positioning information.

NovacoHub is a discreet plug-and-play solution that is fitted to the wheelhouse and can be connected simply via a single Ethernet cable to bridge systems. The vessel benefits from secure navigation data delivery, removing the security and virus risk of DVDs and USB sticks. <https://shipinsight.com>

---

### Mapping services for autonomous driving

Luokung Technology Corp, China has announced that its previously announced acquisition candidate, eMapgo Technologies (Beijing) Co., Ltd. (“EMG”) and Beijing New Energy Automobile Co., Ltd. (BAIC BluePark New Energy Technology Co., Ltd. have agreed to collaborate on the development of autonomous driving projects for BAIC BJEV’s electric vehicles (EVs).

EMG recently worked with BAIC BJEV to provide HD map services in autonomous valet parking (“AVP”) for BAIC New Energy vehicles. The two parties will cooperate in depth on L3 (conditional driving automation) to L4 (high driving automation) autonomous driving related projects. [www.luokung.com](http://www.luokung.com)

---

### Smartphone app for facial recognition by Australian Govt.

The State Government announced a contract to a Western Australian (WA) company for \$1.1 million to develop a new smartphone app that uses facial recognition and GPS tracking technology to monitor people who are ordered to self-quarantine at home. It would be used to track people who arrive in South Australia from interstate COVID-19 hotspots, or who are close or casual contacts of local cases, to ensure that they comply with quarantine directions. <https://indaily.com.au> 

---

### Tallysman introduces the HC843 and HC843E lightweight dual-band GNSS

Tallysman® Wireless Inc. announced the addition of two new models to its industry-leading line of Helical antennas.

The key feature of the HC843 and HC843E is their two-mode operation. The first mode is dual-frequency GNSS and the second is passive Iridium™ (1616.0 – 1626.5 MHz), which supports both voice and data communications. The antenna operates in GNSS mode when its input voltage is less than 5.5 VDC, and in Iridium mode when it is more than 5.5 VDC.

The HC843 housed and HC843E embedded helical antennas are designed and built for high-accuracy positioning in a very light and compact form factor. Both models support GPS/QZSS-L1/L2, GLONASS-G1/G2, Galileo-E1, and BeiDou-B1, including WAAS (North America), EGNOS (Europe), MSAS (Japan), and GAGAN (India). [www.tallysman.com](http://www.tallysman.com)

---

### Trimble teams with ROBORACE

Trimble and ROBORACE, the world’s first autonomous racing series with electric-powered vehicles, announced recently a comprehensive technology and marketing alliance. As part of the alliance, ROBORACE will utilize Trimble’s Applanix POS LVX™ GNSS-inertial systems in its next-generation autonomous race cars for Season 1 of the championship, which begins in September 2021. [www.trimble.com](http://www.trimble.com)

---

### Longest and deepest alternating current cable route surveyed

A two-person Astrolabe Engineering survey team using a single SP60 GNSS receiver recently completed the entire land and sea route for the world’s longest and deepest alternating current (AC) cable.

Linking the island of Crete to mainland Greece, the 174-kilometer-long interconnection, of which 132 kilometers

are on the seabed, became fully functional last month. Connecting Megalopolis in central Peloponnese with Heraclion, the biggest city on the island, the cable is expected to meet more than a third of the island’s electrical power demand and enable the island to permanently close its most polluting power plants.

The European Union funded project, managed by Independent Power Transmission Operator (IPTO), selected AstroLabe Engineering to perform the survey. The land portion was a topographic survey stake-out of the center line and boundaries of the corridor to be trenched as well as a topographic record of the trench depth and exact cable location in the trench. The marine portion was marked using Differential Global Positioning System (DGPS), survey lines and markers with buoys close to shore on both the mainland and Crete. During backfilling an additional topographic survey recorded the profile of the installed cable. [spectrageopsatial.com](http://spectrageopsatial.com)

---

### Sonardyne’s SPRINT-Nav reaches new heights of capability

Sonardyne has released a new high altitude variant of its market leading hybrid navigator SPRINT-Nav to allow uncrewed surface vessels (USVs) and underwater vehicles to extend their operational envelope.

SPRINT-Nav tightly integrates a Sonardyne SPRINT INS, Syrinx DVL and a highly accurate pressure sensor into a single high-performance solution providing navigation and optional acoustic Doppler current profile (ADCP) functionality. [www.sonardyne.com](http://www.sonardyne.com)

---

### Trimble SX12 scanning total station

Trimble has introduced the Trimble® SX12 Scanning Total Station, the next iteration of its breakthrough 3D scanning total station that provides fast and efficient data capture for surveying, engineering and geospatial professionals. New features, including a high-power laser pointer and high-resolution camera system, expand

capabilities in surveying and complex 3D modeling and enable new workflows in tunneling and underground mining.

The Trimble SX12 merges high-speed 3D laser scanning, Trimble VISION™ imaging technology and high-accuracy total station measurements into familiar field and office workflows for surveyors. A new green, focusable Class 1M laser pointer is safe for viewing with the naked eye, offers high-power visibility and makes it easy to see even at a distance. An improved camera system provides enhanced pointing and site documentation capabilities. [www.trimble.com](http://www.trimble.com)

---

### Momentum service agreement with Xona Space Systems

Momentum Inc. a commercial space company offering in-space infrastructure services, and Xona Space Systems, a San Mateo-based startup creating a secure and precise Position, Navigation, and Timing (PNT) satellite service, announced a service agreement to advance Xona's 2022 Alpha mission.

Xona's patent-pending system architecture is combining the efficiency and innovation of the new space era with the world of satellite navigation to help enable modern intelligent systems to operate safely in any conditions, anywhere on the planet. Once complete, their low Earth orbit smallsat constellation will provide a resilient alternative to Global Navigation Satellite Systems (GNSS) with more than 10x better accuracy. [www.momentum.space](http://www.momentum.space)

---

### European Commission awards H2020 Grant

GMV has been chosen by the European Commission to lead a Coordination and Support Action (CSA) within the H2020 program to make proposals for a future European Space Traffic Management (STM) capability: EUSTM.

Space activity has increased exponentially in recent decades. The number of objects in orbit is likely to increase drastically, and it is therefore necessary to develop

capabilities to manage them in an efficient manner. An increasing need for a policy and legal framework supported by the required technology developments has also emerged to foster and ensure the desired security, safety, sustainability, and stability of space operations. These frameworks are broadly known as Space Traffic Management (STM) while the technology supporting is referred to as Space Situational Awareness (SSA) or Space Surveillance and Tracking (SST).

In Europe, the SSA/SST remit is held by ESA and the European Commission. SSA/SST activities are currently focused on creating an architecture of radars, telescopes, SLR stations and data centers dedicated to the surveillance and protection of space infrastructure. [www.gmv.com](http://www.gmv.com)

---

### Swift Navigation raises \$50 million

Swift Navigation has announced that it has raised a \$50 million Series C round of financing led by existing investors Forest Baskett and Greg Papadopoulos of New Enterprise Associates (NEA), existing investor Eclipse Ventures and new investors, including EPIQ Capital Group and KDDI Open Innovation Fund.

Swift offers a comprehensive GNSS platform, consisting of the receiver-agnostic Starling® software positioning engine that easily integrates with the automotive sensor suite and pulls centimeter-accurate location corrections from Skylark™—Swift's wide area, cloud-based GNSS precise positioning service. [swiftnav.com](http://swiftnav.com)

---

### ACEINNA OpenRTK330LI EVK, a development kit

ACEINNA has announced the general market availability of ACEINNA OpenRTK330LI EVK, a complete evaluation and development kit for the OpenRTK330LI GNSS/INS module. The OpenRTK330LI EVK accelerates development and reduces time to market of custom navigation and guidance systems fusing inertial measurements

and multi-band RTK/GNSS positioning. The OpenIMU330LI Module is a very compact, low cost, state-of-the-art, high performance RTK/GNSS receiver with built-in triple redundant inertial sensors. [www.aceinna.com](http://www.aceinna.com)

---

### Teledyne CARIS receives Canada's Ocean Supercluster award

Teledyne CARIS has announced significant funding from Canada's Ocean Supercluster award to develop software for remote operations survey processing. This is in alignment with the company's leading AI strategy. The company has partnered with Ocean Floor Geophysics (OFG), a pioneering CARIS customer. In addition to OFG, Teledyne CARIS will be working with other stakeholders to assist on training, including the University of New Brunswick and Memorial Universities Marine Institute. [teledyne.com](http://teledyne.com)

---

### Honeywell successfully completes in-flight demonstration of M-Code

Honeywell has successfully flight-tested new technologies designed to enable alternative navigation offerings, including its Embedded GPS Inertial Navigation System (EGI) supporting M-code, the new standard GPS signal used by militaries around the world. These tests, which involved equipping a Honeywell test aircraft with alternative navigation technologies, demonstrate a major milestone in providing continued navigation solutions in GPS-denied environments. This was also the first time an airborne M-code receiver was flown on an aircraft in an EGI, demonstrating the effectiveness of M-code in a live, airborne environment.

Around the world, GPS signals are used for navigation in commercial and military applications alike, but seamless connection to these signals is not always guaranteed. Even modern systems can have problems in "GPS-denied" environments like dense urban areas near tall buildings or under bridges. Furthermore, GPS-jamming, whether intentional or not, can prevent these vital signals from conveying critical

information regarding positioning, navigation and timing. In these instances, it is also important for vehicles and aircraft to be equipped with alternative navigation technologies, like celestial or vision navigation. [aerospace.honeywell.com](http://aerospace.honeywell.com)

---

## STMicroelectronics simplifies portable GNSS receivers

STMicroelectronics' BPF8089-01SC6 RF front-end for Global Navigation Satellite System (GNSS) receivers simplifies design and saves real-estate by integrating the impedance-matching and electrostatic-discharge (ESD) protection circuitry typically implemented using discrete components.

The BPF8089-01SC6 provides a 50Ω matched interface between the receiver's antenna and low-noise amplifier (LNA), and is ready to plug-and-play with ST's STA8089 and STA8090 LNAs. This compact, integrated device typically replaces a matching network containing up to five capacitors, resistors, and inductors, as well as two discrete protection devices, resulting in a much smaller footprint. Designers can also leverage PCB-track specifications provided in the device datasheet to ease design challenges and ensure optimal performance.

The ESD protection provided complies with IEC 61000-4-2 (C = 150pF, R = 330Ω) and exceeds level 4: 8kV for contact discharge and 15kV for air discharge. The device also withstands 2kV pulse voltage in accordance with MIL STD 883C (C = 100pF, R = 1.5kΩ). [www.st.com](http://www.st.com)

---

## GNSS receiver with open software interface

TeleOrbit, Germany, has implemented testing capability for Galileo's Open Service Navigation Message Authentication (OSNMA) aboard the company's GNSS Receiver with Open Software Interface (GOOSE).

As the threat of GNSS spoofing continues to grow, authentication of

signals represents a safeguard for industry, vital infrastructure and safety-critical GNSS applications, including autonomous vehicles. As yet there is no authentication service available, but Galileo will be first to the market with scheduled launch in 2023.

TeleOrbit's GOOSE platform is an FPGA-based GNSS receiver, characterized by four separate components: a multi-frequency GNSS antenna, an analog front-end board, a baseband board, and the processor system. It grants deep access to the hardware interface, down to integrate and dump value levels, according to the company. Intermediate frequency signals can be recorded, processed and replayed with the platform. <https://teleorbit.eu>

---

## Pipistrel selects C-Astral Aerospace

Pipistrel is relaunching the NUUVA V20 based on initial customer feedback and needs. It is gaining capability that goes beyond delivery of cargo such as spare parts, valuable items, medical supplies etc., by adding ISR functionality with a diverse array of payloads, sensors and data link options for achieving superior situational awareness and C4I systems integration.

Pipistrel is excited to partner with C-ASTRAL Aerospace, whose UAS integration and R&D experience will enrich the product with proven and class-leading C4 solutions intuitive ground station elements and support suites. [www.c-astral.com](http://www.c-astral.com)

---

## eBee Ag Fixed-wing Mapping Drone for Agriculture

senseFly announced the launch of eBee Ag, the latest addition to the eBee X series of drone solutions. It helps agriculture professionals overcome the many challenges they face in the field related to planning, plant health and crop monitoring. eBee Ag makes it easier than ever to field scout, ground-truth potential problem areas and gain critical crop health and field information.

Equipped with its standard battery, it is capable of up to 45-minutes of flight. An endurance battery increases flight times to up to 55 minutes—allowing eBee Ag to cover more than 160 hectares (395 acres) in a single flight and saving precious time and money when compared with conventional scouting. [www.sensefly.com](http://www.sensefly.com)

---

## ArcGIS Velocity by Esri

Esri has released ArcGIS Velocity. Previously known as ArcGIS Analytics for IoT, it is a new cloud-native capability for ingestion, processing, visualization, and analysis of real-time and high-volume geospatial data on the fly. It complements existing systems with GIS technology by spatially enabling the Internet of Things (IoT) data from current providers and simplifying real-time data analysis.

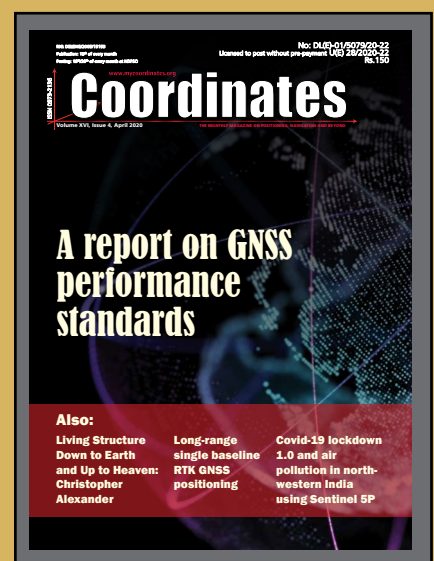
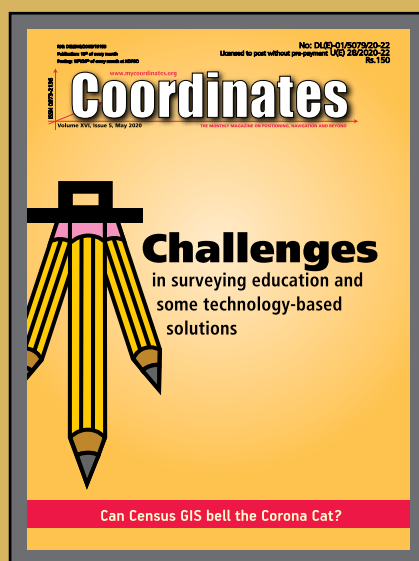
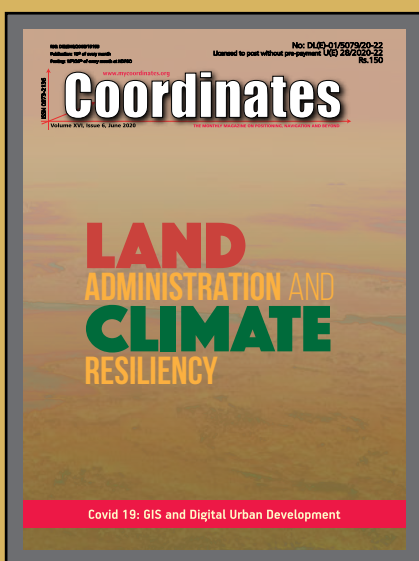
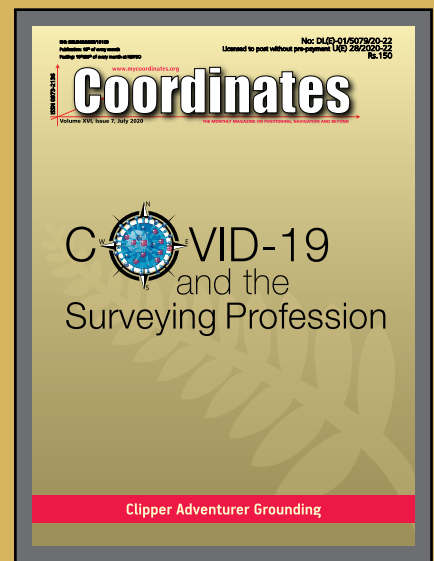
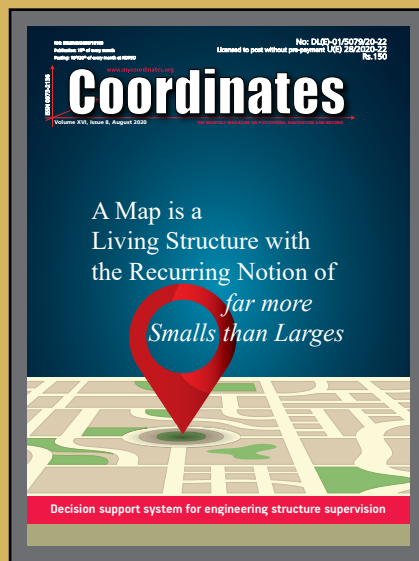
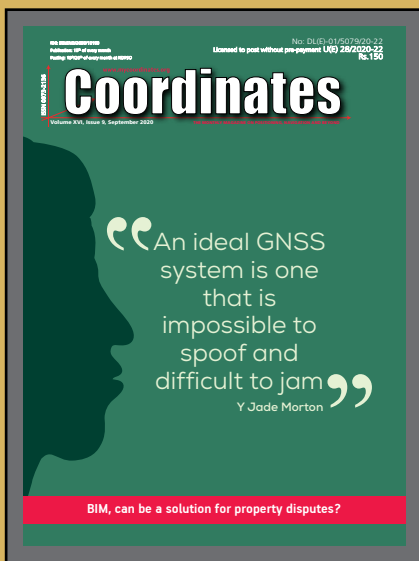
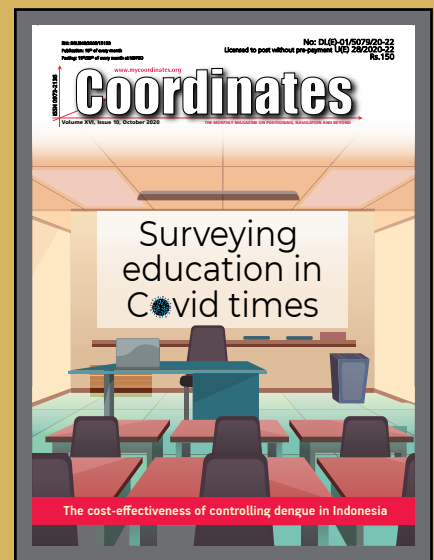
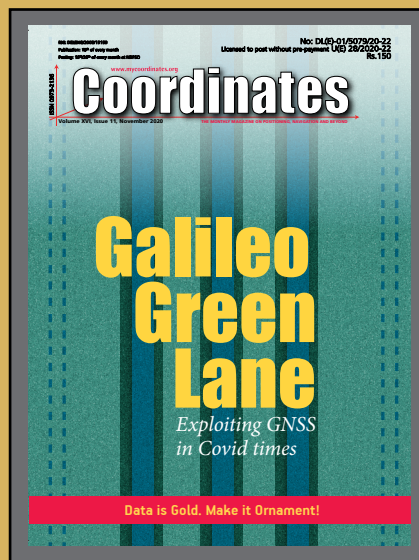
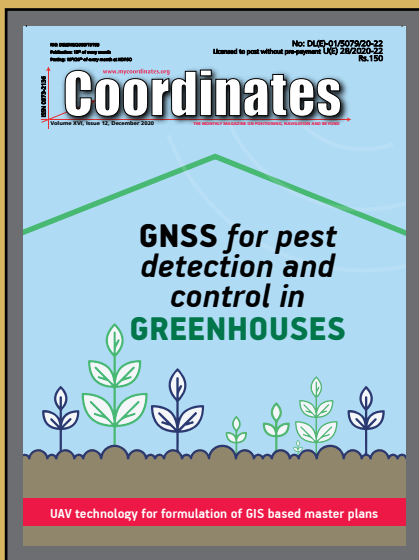
---

## MAPPS 2020 Geospatial Excellence Awards for UltraCam Osprey 4.1

At the MAPPS 2021 Winter Conference in Orlando, Florida, Vexcel Imaging was presented with two separate awards for its Osprey 4.1 nadir/oblique aerial camera system released in the second half of 2020.

The Geospatial Excellence Awards are presented to Regular and Associate Member firms whose entries exemplify the professionalism, value, integrity and achievement of the firm's staff as demonstrated over the previous year. A distinguished and impartial panel of two judges evaluated the submitted projects from five categories: Data Acquisition & Processing, Surveying/Field Data Collection, GIS/IT/Remote Sensing Analysis, Small Projects (no entries were submitted for this category), and Technology Innovation/Licensed Data Products. A winner was selected for each category with submissions.

Vexcel Imaging received awards for its Osprey 4.1 under the Technology Innovation/Licensed Data Products category and additionally received the Grand Award – Project of the Year. [www.vexcel-imaging.com](http://www.vexcel-imaging.com) 



**“The monthly magazine on Positioning, Navigation and Beyond”**  
 Download your copy of Coordinates at [www.mycoordinates.org](http://www.mycoordinates.org)



## Need a portable GNSS testing solution? Work anywhere with LabSat

LabSat GNSS simulators are lightweight, portable and affordable – making them your ideal test partner anywhere you need to work.

- Multi-Constellation
- Multi-Frequency
- One-touch Record & Replay
- SatGen simulation software
- From only \$4,990



LabSat GNSS simulators – Test Anywhere

[labsat.co.uk](http://labsat.co.uk)